Climate and Land Cover Trends Affecting Freshwater Inputs to a Fjord in Northwestern Patagonia

Jorge León-Muñoz, Rodrigo Aguayo, Rafael Marcé, Núria Catalán, Stefan Woelfl, Jorge Nimptsch, Ivan Arismendi, Camila Contreras, Doris Soto, Alejandro Miranda

frontiers in Marine Science

ORIGINAL RESEARCH
published: 20 July 2021
doi: 10.3389/fmars.2021.628454

Climate and Land Cover Trends Affecting Freshwater Inputs to a Fjord in Northwestern Patagonia

Jorge León-Muñoz[1,2], Rodrigo Aguayo[3], Rafael Marcé[4,5], Núria Catalán[5,6,7], Stefan Woelfl[8], Jorge Nimptsch[8], Ivan Arismendi[9], Camila Contreras[10], Doris Soto[2] and Alejandro Miranda[11,12]*

[1] Departamento de Química Ambiental, Facultad de Ciencias, Universidad Católica de la Santísima Concepción, Concepción, Chile, [2] Centro Interdisciplinario para la Investigación Acuícola (INCAR), Concepción, Chile, [3] Facultad de Ciencias Ambientales, Centro EULA, Universidad de Concepción, Concepción, Chile, [4] Catalan Institute for Water Research (ICRA), Scientific and Technological Park of the University of Girona, Girona, Spain, [5] Universitat de Girona, Giona, Spain, [6] United States Geological Survey, Boulder, CO, United States, [7] Laboratoire des Sciences du Climat et de l'Environnement, LSCE, CEA, CNRS, UVSQ, Gif-sur-Yvette, France, [8] Facultad de Ciencias, Instituto de Ciencias Marinas y Limnológicas, Universidad Austral de Chile, Valdivia, Chile, [9] Department of Fisheries, Wildlife and Conservation Sciences, Oregon State University, Corvallis, OR, United States, [10] Departamento de Ingeniería Civil y Ambiental, Facultad de Ingeniería, Universidad del Bío-Bío, Concepción, Chile, [11] Laboratorio de Ecología del Paisaje y Conservación, Departamento de Ciencias Forestales, Universidad de La Frontera, Temuco, Chile, [12] Center for Climate and Resilience Research (CR2), Santiago, Chile

OPEN ACCESS

Edited by:
Brian Reid, Patagonian Ecosystems Investigation Research Center (CIEP), Chile

Reviewed by:
Vanesa Magar, Center for Scientific Research and Higher Education in Ensenada (CICESE), Mexico
Facundo Scordo, University of Nevada, Reno, United States

***Correspondence:**
Jorge León-Muñoz
jleon@ucsc.cl

Specialty section:
This article was submitted to Coastal Ocean Processes, a section of the journal Frontiers in Marine Science

Received: *12 November 2020*
Accepted: *28 June 2021*
Published: *20 July 2021*

Citation:
León-Muñoz J, Aguayo R, Marcé R, Catalán N, Woelfl S, Nimptsch J, Arismendi I, Contreras C, Soto D and Miranda A (2021) Climate and Land Cover Trends Affecting Freshwater Inputs to a Fjord in Northwestern Patagonia. Front. Mar. Sci. 8:628454. doi: 10.3389/fmars.2021.628454

Freshwater inputs strongly influence oceanographic conditions in coastal systems of northwestern Patagonia (41–45°S). Nevertheless, the influence of freshwater on these systems has weakened in recent decades due to a marked decrease in precipitation. Here we evaluate potential influences of climate and land cover trends on the Puelo River (640 m^3s^{-1}), the main source of freshwater input of the Reloncaví Fjord (41.5°S). Water quality was analyzed along the Puelo River basin (six sampling points) and at the discharge site in the Reloncaví Fjord (1, 8, and 25 m depth), through six field campaigns carried out under contrasting streamflow scenarios. We also used several indicators of hydrological alteration, and cross-wavelet transform and coherence analyses to evaluate the association between the Puelo River streamflow and precipitation (1950–2019). Lastly, using the WEAP hydrological model, land cover maps (2001–2016) and burned area reconstructions (1985–2019), we simulated future land cover impacts (2030) on the hydrological processes of the Puelo River. Total Nitrogen and total phosphorus, dissolved carbon, and dissolved iron concentrations measured in the river were 3–15 times lower than those in the fjord. Multivariate analyses showed that streamflow drives the carbon composition in the river. High streamflow conditions contribute with humic and colored materials, while low streamflow conditions corresponded to higher arrival of protein-like materials from the basin. The Puelo River streamflow showed significant trends in magnitude (lower streamflow in summer and autumn), duration (minimum annual streamflow), timing (more floods in spring), and frequency (fewer prolonged floods). The land cover change (LCC) analysis indicated that more than 90% of the basin area maintained its land cover, and that the main changes were attributed to recent large wildfires. Considering these land cover trends, the hydrological simulations

project a slight increase in the Puelo River streamflow mainly due to a decrease in evapotranspiration. According to previous simulations, these projections present a direction opposite to the trends forced by climate change. The combined effect of reduction in freshwater input to fiords and potential decline in water quality highlights the need for more robust data and robust analysis of the influence of climate and LCC on this river-fjord complex of northwestern Patagonia.

Keywords: Patagonia, climate change, hydrological modeling, water quality, land-ocean interface, land cover change

INTRODUCTION

The land-ocean interface in river deltas and fjords is the natural bridge between terrestrial and marine systems. In these areas, nutrients, organic matter and sediments transported by rivers meet with those coming from the coastal and open ocean. Globally, oceans receive more than 36,000 km^3 of freshwater and about 20 billion tons of sediments (Milliman and Farnsworth, 2011). About 95% of this volume enters through the rivers. The freshwater input represents important regulating and provisioning ecosystem services, influencing the coastal system's physical-chemical characteristics, supporting the reproduction of numerous species, many of which sustain important fisheries and subsistence activities (Nixon and Buckley, 2002; Barbier et al., 2011).

The coastal system of Northwestern Patagonia (41–45°S) is comprised by extensive and interconnected fjords, bays and channels that receive important freshwater inputs from the southern Andes Range (Milliman and Farnsworth, 2011; Pantoja et al., 2011; Iriarte et al., 2014). Most of the freshwater inputs come from numerous rivers that are fed by rainfall runoff, snow melt and glacier melt from relatively small basins ($<$ 10,000 km^2). Freshwater inputs influence the coastal dynamics at different spatial and temporal scales, producing marked density gradients in the seawater column (Dávila et al., 2002; Saldías et al., 2019), changing nutrient ratios, and bringing high concentrations of organic matter (dissolved and particulate) and silicic acid (Silva et al., 2011; Vargas et al., 2011; Torres et al., 2020). Inorganic nutrients and solar radiation are strongly seasonal, limiting the relatively high primary productivity of estuarine systems in western Patagonia (0.5–3.0 g C m^{-2} d^{-1}) dominated mainly by diatoms (90%) (Iriarte et al., 2007; Jacob et al., 2014; Raymond and Spencer, 2015). Changes in freshwater input could have negative implications on oceanographic processes to fjords in the inner seas of Chilean Patagonia. The ecosystem services that these systems provide depend on the interplay of different water masses, especially including the upper estuarine layer (Sievers and Silva, 2008), which strongly depends on the magnitude, timing, and duration of freshwater input. The depth, extent and chemistry of this layer/water mass also depends on the complexity of processes occurring at the climate-dependent river-ocean interface.

The influence of rivers on the coastal systems in this region has weakened during the last decades (León-Muñoz et al., 2018; Aguayo et al., 2019, 2021) due to a marked decrease in precipitation during summer and autumn (Boisier et al., 2018). The precipitation decline has been attributed to the positive trend of the Southern Annular Mode (SAM), an index that describes the movement of the low-pressure belt that generates westerly winds. The SAM trend has been attributed to stratospheric ozone depletion and increased greenhouse gases concentration, which suggests the effects of a global anthropogenic forcing on the local precipitation regime (Arblaster and Meehl, 2006; Eyring et al., 2013; Boisier et al., 2018). This trend has increased the climate synergy with El Niño-Southern Oscillation (ENSO), promoting severe droughts during austral summers (Garreaud, 2018). Climate projections for the next decades (2020–2070) follow this trend. Recent studies have evaluated the hydrological impacts of climate projections in the region (Puelo River; 41°S) predicting a prolongation of warm and dry conditions, seasonal changes in hydrological regimes and an increase in severe drought frequency (Aguayo et al., 2019, 2021; Pessacg et al., 2020).

Apart from shifts in climate conditions, the magnitude and spatial expansion of land cover changes (LCC) may strongly alter river hydrology (Ellison et al., 2017) and biogeochemistry (Cuevas et al., 2006; Raymond et al., 2008; Aufdenkampe et al., 2011), and thus their influence on the coastal systems. A large proportion of native forest cover has been identified as a factor providing resilience to coastal systems strongly influenced by freshwater against climate change (Desmit et al., 2018; Khoury and Coomes, 2020). Native forest substitution by exotic tree plantations in south-central Chile (34–41°S; Miranda et al., 2017; Uribe et al., 2020) has been identified as one of the causes of lower streamflow during summer (Little et al., 2009; Iroumé and Palacios, 2013; Alvarez-Garreton et al., 2019). Climate change has also increased the recurrence of wildfires in this region (Urrutia-Jalabert et al., 2018), which could potentially alter hydrological processes (Rulli and Rosso, 2007; Boisramé et al., 2019). The impact of LCC on riverine biogeochemistry can affect nutrients and carbon cycling. Dissolved organic matter (DOM) composition is strongly influenced by land cover. For example, different types of vegetation reflected as divergent biomarkers in coastal waters (Hernes and Benner, 2003; Raymond and Spencer, 2015).

Anthropogenic alterations of the natural streamflow regime by way of LCCs make isolating the impacts of climate change on hydrology a daunting task (Yang et al., 2017; Chanapathi and Thatikonda, 2020). In Chile the hydrological impacts of LCCs have been evaluated mainly in south-central Chile ($<$ 41°S; Stehr et al., 2010; Aguayo et al., 2016; Martínez-Retureta et al., 2020;

Barría et al., 2021; Galleguillos et al., 2021) and not in tributary basins to the coastal system of northwestern Patagonia. Nevertheless, using rivers like Puelo River as sentinels, several studies have reported anomalous events in fjords of northwestern Patagonia (e.g., surface hypoxia events, harmful algal blooms), mainly during severe droughts (Valle-Levinson et al., 2007; León-Muñoz et al., 2013, 2018; Iriarte et al., 2017; Díaz et al., 2021). Although northern Patagonian basins have not yet been modified by irrigation channels or reservoirs and still maintain extensive little-degraded native forest cover (CONAF and UACH, 2014; Astorga et al., 2018), recent threats such as increased wildfires and their joint effect with climate change have not been evaluated hydrologically to date. Considering this context, here we evaluate the influence of climate and land cover trends on the freshwater inputs of the Puelo River Basin to the Reloncaví Fjord (41.5°S; **Figure 1**). Specifically, we aim to 1) characterize the water quality of freshwater inputs along the Puelo River network and the Reloncaví Fjord (2018–2019), 2) evaluate trends in natural flow regime (1950–2019), precipitation-streamflow associations (1950–2019), and land cover (2001–2016) for the Puelo River Basin, and 3) estimate the potential future impacts of LCC (2030), mainly caused by forest fires, on the hydrological processes of the Puelo River.

MATERIALS AND METHODS

Study Area

The study area comprises the Puelo River Basin and the Reloncaví Fjord (**Figure 1**). The basin (∼9,000 km^2; 66% of its drainage area in Argentina and 34% in Chile) is located in the central latitudes covered by the Valdivian Rainforest ecoregion. An important part of the basin is covered by native forest (CONAF and UACH, 2014), with minimal anthropogenic interventions (24% of the basin is located in protected areas). According to Köppen-Geiser's classification, the basin has temperate and polar climates with tundra characteristics (Beck et al., 2018). The precipitation range follows a strong longitudinal gradient that can vary between 500 mm and 4700 mm per year (Lara et al., 2008; Aguayo et al., 2019). Half of annual precipitation is concentrated during the austral winter. Recently, Aguayo et al. (2021) determined that the Puelo River Basin has a low aridity index (< 1), suggesting that it is energy-limited. The same basin showed, on average, an evaporation index close to 0 during all seasons except in summer, where evapotranspiration represents 37% of precipitation.

The Puelo River has a mean streamflow of 640 m^3 s^{-1} (2400 mm yr^{-1}) with a pluvial-nival hydrological regime in the proximity of its mouth, with a maximum peak in winter and a second and lower peak during spring (León-Muñoz et al., 2013). In contrast, the sub-basins located at higher elevations have a nival-pluvial hydrological regime. Puelo River is classified as a high-runoff river (>750 mm yr^{-1}); it has one of the highest runoff levels in mesoscale basins (Milliman and Farnsworth, 2011). During austral summer and autumn (low-flow season), the streamflow of the Puelo River is significantly correlated with the streamflow of other rivers of northwestern Patagonia ($r > 0.4$; Lara et al., 2008).

The Puelo River is the main source of freshwater input of the Reloncaví Fjord, the northernmost fjord on Chile's coast and one of the coastal systems most intensively used for aquaculture in the last decades. Chile is one of the world's 10 top aquaculture producers, the second-largest exporter of salmon and trout, and the largest exporter of mussel (*Mytilus chilensis*). The Reloncaví Fjord has historically been used for smoltification and growth of salmonids by industrial salmon farming (Quiñones et al., 2019; Soto et al., 2019). This fjord is also essential for the seed production of Chilean mussel farming (Molinet et al., 2015). The fjord has a J-shape; it is 55 km long and less than 3 km near the head. The bathymetry of the Reloncaví Fjord shows depths >400 m in the area close to the mouth with a deep sill (∼ 150 m depth) located 15 km inland (Valle-Levinson et al., 2007). This fjord has a three-layer circulation pattern with an upper brackish layer flowing into the mouth and is strongly associated with freshwater inputs from the Puelo River and other tributaries (Cochamoì River Q = 100 m^3 s^{-1}; Petrohueì River Q = 250 m^3 s^{-1}). The system's stratification varies along the fjord and between seasons, decreasing toward the mouth and being maximum in winter. The Reloncaví Fjord has been extensively studied by several research projects, mainly oceanographic, including paleoclimate (Rebolledo et al., 2015), fjord hydrodynamics (Valle-Levinson et al., 2014; Castillo et al., 2016), fjord biogeochemistry (Farías et al., 2017; González et al., 2019; Vergara-Jara et al., 2019; Yevenes et al., 2019) and plankton biology (González et al., 2013; Iriarte et al., 2017).

Data

Hydrology and Climate

Daily instrumental data of precipitation, air temperature, and streamflow were obtained from the Dirección General de Aguas de Chile, Dirección Meteorológica de Chile, Subsecretaría de Recursos Hídricos de Argentina and the Servicio Meteorológico Nacional de Argentina. According to these records, the Puelo River Basin contains one of the largest and most extensive networks of stations in western Patagonia. However, the location of the stations is spatially heterogeneous (**Figure 1**). Given this limitation, precipitation and temperature monthly data were complemented with CHIRPSv2 (2000–2019; 0.05°; Funk et al., 2015) and MODIS MOD11C3 (2000–2019; 0.05°; Wan et al., 2015) products, respectively. The associated biases between instrumental data and gridded products were corrected with different methodologies detailed in Aguayo et al. (2019). Wind and relative humidity monthly data were directly obtained from the ERA5 atmospheric reanalysis (2000–2019; 0.25°; Hersbach et al., 2020).

Water Quality

Six sampling sites were chosen within the drainage network to characterize the water quality of the Puelo River (**Figure 1** and **Table 1**). Sampling sites were located downstream of Lake Inferior (P1), before and after (P2, P3) the confluences with its main tributaries, the Ventisquero (V1) and Manso (M1) rivers, and downstream of Lake Tagua-Tagua (P4) before its discharge in the Reloncaví Fjord (**Figure 1**). One additional sampling site was established in the Reloncaví Fjord near the Puelo River

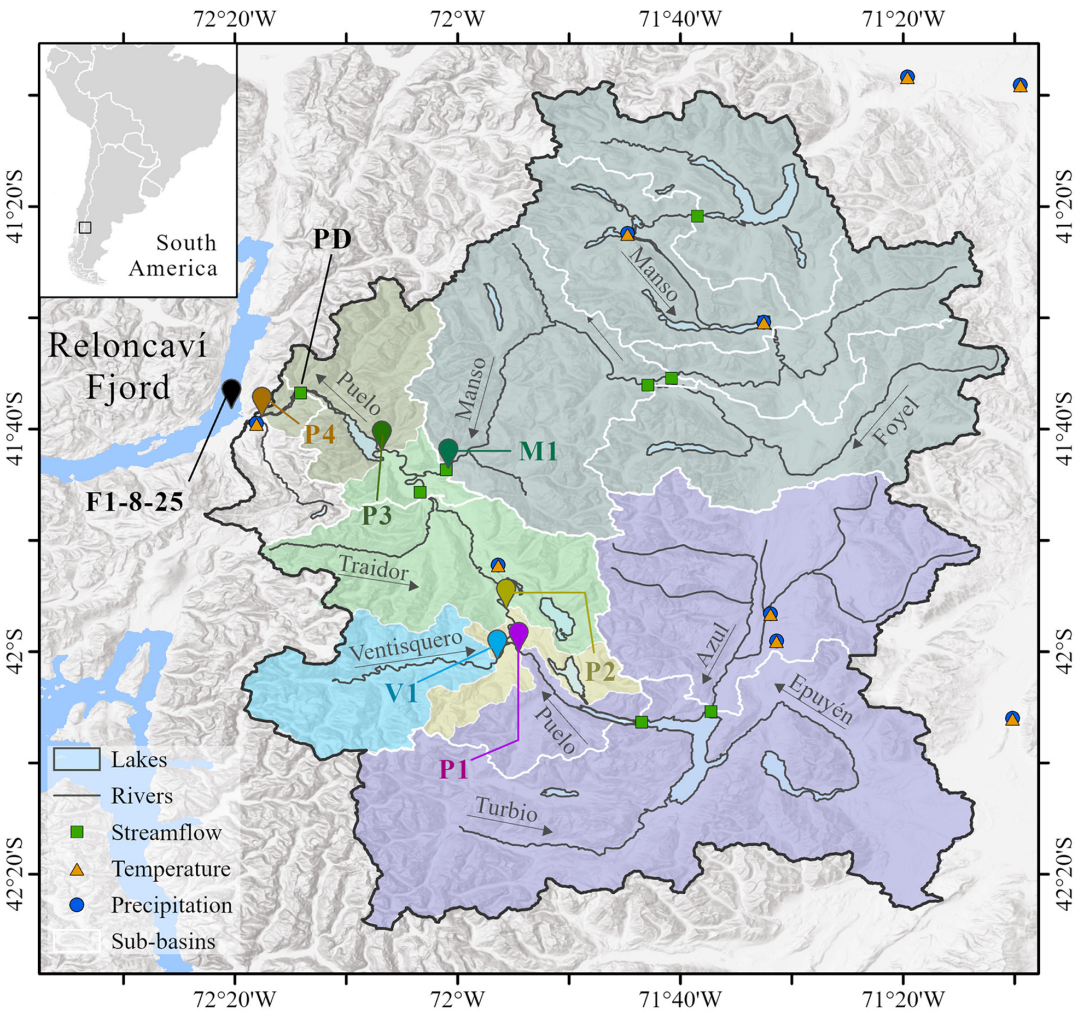

FIGURE 1 | Study area composed of the Puelo River Basin and the Reloncaví Fjord. Within the basin, the names and arrows indicate the principal rivers of the Puelo River drainage network. Geometric symbols indicate the fluviometric and meteorological stations used in the study. Vignettes indicate the sampling points in the Puelo River drainage network (P1, P2, P3, P4, V1 and M1) and Reloncaví Fjord (F; depths 1, 8, and 25 m). The colored polygons represent the sub-basins for each sampling point. The white lines indicate the sub-basins used in the hydrological modeling (section "Hydrologic Modeling of LCC").

mouth (**Figure 1** and **Table 1**). At this site the samples were extracted at 1, 8, and 25 m depth. The 1 m depth sample was intended to represent the upper brackish layer of the fjord (strong freshwater influence). The 25 m depth sample was designed to represent the fjord's middle layer (below the pycnocline). Finally, the 8 m depth sample aims to reflect the seasonal changes in the system stratification, which, as mentioned, is highly dependent on freshwater inputs and other forcing factors such as tides and wind (Valle-Levinson et al., 2014; Castillo et al., 2016). According to continuous measurements carried out between May and September, 2018 these depths presented mean salinity values of 7, 28 and 30, respectively. Each sampling site was visited six times between 2018 and 2019 (42 site-date combinations). The timing of each field campaign was determined based on the monthly Flow Duration Curve (FDC) of the Puelo River during the period 1990–2019 (**Figure 2**). Considering the distance between sampling sites and the characteristics of the study area (**Figure 1**), each campaign was sampled within 3 days, which allowed capturing the variability of short-term events such as floods (**Figure 2**).

The water samples collected in field campaigns were used to analyze nutrients ($N\text{-}NH_4$, $N\text{-}NO_3$, $N\text{-}NO_2$, N-TOTAL, $P\text{-}PO_4$, P-TOTAL), dissolved organic and inorganic carbon concentration (i.e., DOC and DIC), DOM optical spectroscopy, and dissolved iron. For nutrient analysis, the water samples were collected (0.25 L) and stored at −18°C for further analysis according to standard methods established by American Public Health Association, 2005 in the Institute of Marine and Limnological Sciences, Faculty of Sciences, Universidad Austral de Chile.

$N\text{-}NO_3$ was determined by the cadmium reduction method (APHA 4500-E), whereas $N\text{-}NO_2$ by diazotizing with sulfanilamide and coupling with N-(1-naphthyl)-ethylenediamine dihydrochloride (APHA 4500-NO_2 – B).

TABLE 1 | Biophysical attributes of each sub-basin delimited by the sampling points within the Puelo River Basin (**Figure 1**).

		P1	P2	P3	P4	M1	V1
General attributes	Area (km^2)	3,455	4,116	8,497	8,936	3,591	460
	Mean elevation (m)	1,022	1,029	1,078	1,067	1,186	1,149
	Mean slope (deg)	21.8	22.6	22.8	23.1	22.3	29.2
	Mean snow cover extent (%)	36%	38%	36%	36%	34%	54%
	Lakes (km^2)	79.3	96.9	212.7	230.6	91.4	4.3
	Mean annual precipitation (mm)	1,890	2,280	2,400	2,550	2,070	4,800
	Mean annual air temperature (°C)	6.4	6.3	5.8	5.8	4.9	4.8
Burned area (km^2)	Total area	485.9	497.7	592.0	630.0	48.8	11.0
	1990–1999	100.2	111.2	187.1	224.9	38.6	11.0
	2000–2009	121.1	121.1	139.2	139.2	8.9	0.0
	2010–2019	166.4	166.4	166.4	166.4	0.0	0.0
Land cover 2001 (%)	Primary forest	18%	19%	24%	25%	26%	16%
	Secondary forest	2%	3%	3%	3%	3%	8%
	Stunted forest	22%	20%	27%	26%	36%	7%
	Exotic tree plantation	0.1%	0.09%	0.05%	0.05%	0.03%	0.0%
	Shrubland	19%	18%	14%	14%	11%	13%
	Grassland	6%	5%	4%	4%	3%	2%
	Urban	0.12%	0.1%	0.05%	0.05%	0.0%	0.0%
	Water body	2.4%	2.4%	2.6%	2.7%	2.6%	1.0%
	Snow and ice	7%	9%	6%	6%	3%	23%
	Bare land	23%	23%	19%	19%	16%	29%

*The water quality sampling points were located downstream of Lake Inferior (P1), before and after (P2, P3) the confluences with its main tributaries, the Ventisquero (V1) and Manso (M1) rivers, and downstream of Lake Tagua-Tagua (P4), before its mouth in the Reloncaví Fjord (**Figure 1**). Land cover classes are defined in section "Land Cover Change." Reconstruction methods and sources of burned areas are described in section "Wildfires."*

Ammonium was determined by the phenate method (APHA 4500-NH_3 F), total nitrogen was determined by the sodium hydroxide and persulfate digestion method (APHA 4500-N/C) followed by the determination of total N-NO_3. Total phosphorous (Total-P) was measured using the sodium hydroxide and persulfate digestion method (4500-P B/5) followed by the determination of soluble phosphorus using the method of acid ascorbic - blue indophenol (APHA 4500-PE).

Samples for DOC, DIC and DOM quality were filtered (GFF, nominal pore sizes = 0.7 and 0.22 μm) to analyze DOM optical spectroscopy, and DOC replicates were filtered and fixed by adding 100 μL of fuming HCl (Merck) to stop microbial activity, and transported at 4–7°C to the laboratory for subsequent analysis. Note that samples from the deepest point in the fjord (F25) were not available for DOM. DOC concentrations were measured using high-temperature catalytic oxidation (HighTOC, Elementar Systems) as described in Kamjunke et al. (2017). Fluorescence of DOM was measured using a Varian Cary Eclypse fluorescence spectrometer (Santa Clara, CA, United States) as described in Nimptsch et al. (2014). Briefly, excitation matrices from 240 to 450 nm (5 nm steps) and emission from 300 to 600 nm, inner filter corrections and Raman standardization were done using the FDOMcorr toolbox v1.6 for Matlab (Murphy et al., 2010). Parallel Factor Analysis Model (PARAFAC) was performed using DOMFluor toolbox v1.7 for Matlab (Stedmon and Bro, 2008). Four PARAFAC components (i.e. fluorophores C1 to C5) were identified and split-half validated with 1000 iterations with random starts (Stedmon and Bro, 2008).

For the determination of dissolved iron, water samples (volume: 15 ml) were filtered using a 0.2 μm syringe filter and acidified with suprapure nitric acid (MERCK). The samples were analyzed using total-reflection X-ray fluorescence spectrometry (TRXF) following procedures described in Mages et al. (2003). Acidified water samples (10 μl) were prepared onto quartz carriers and internal Ga standard (5 ng, suspended in Suprapur® nitric acid for trace analysis—Sigma-Aldrich) was added. After drying on a hot plate (15 min, 60°C), trace elements were determined using a total reflection X-ray fluorescence spectrometer Picotax (BRUKER).

Land Cover Change

Satellite images were used to analyze the land cover change in the Puelo River Basin. The images were obtained from Landsat 5 and 8 for 2001 (December 16) and 2016 (February 9), respectively. These images have a spatial resolution of 30 m. Using the IDRISI GIS Analysis tool[1], selected images were subjected to standard preprocessing procedure as geometric, radiometric and topographic corrections to reduce the effects of atmosphere and shadows on land surface spectral response (e.g., Echeverria et al., 2006; Fuentes et al., 2017).

The supervised land cover classification of each image was performed in ENVI 4.5 software, which uses maximum likelihood statistics based on training points (Segura and Trincado, 2003). Training point selection for digital supervised classification of the 2001 image were taken from

[1]www.clarklabs.org/terrset/idrisi-gis/

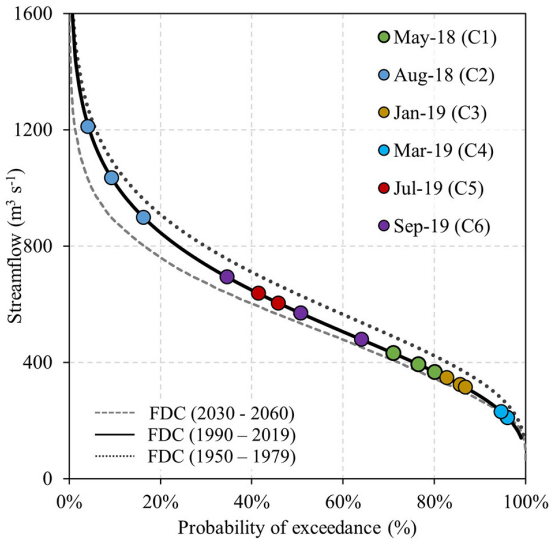

FIGURE 2 | Flow Duration Curve (FDC) of the monthly streamflow of the Puelo River for different periods. The projected streamflows for the period 2030–2060 were obtained from Aguayo et al. (2019). The colors of the circles correspond to the six field campaigns performed in the Puelo River Basin and the Reloncaví Fjord.

CONAF et al. (1999) dataset, a GIS-based data set of thematic maps derived from aerial photographs and satellite imagery from 1998 (Miranda et al., 2018). For the 2016 image classification, 750 training points were obtained from different field campaigns between 2018 and 2019. To increase accuracy of the satellite image classification, the Normalized Difference Vegetation Index (NDVI), Soil Adjusted Vegetation Index (SAVI) and Land Surface Water Index (LSWI) were used as additional spectral bands in both years (Wu et al., 2007).

The spectral information was classified in 10 different land covers categories: primary forests (pristine evergreen forests or those of a natural succession), secondary forest (forests regenerated after a disturbance, whether natural or anthropic), stunted forest (forest under the tree line), exotic tree plantation (commercial plantations mainly of eucalyptus), shrublands, grassland (crop and pastures), urban, water body, snow and ice and bare land. The accuracy assessment consisted of confusion matrices between classified images and independent sampling points collected from aerial photographs and field campaigns. Land cover change analyses were performed using the IDRISI Selva Land Change Modeler module[2]. This analysis consisted of descriptive spatial-temporal statistics of the land covers gains and losses in the time period. The change rates (q) of the different classes were calculated using the equation proposed by Food and Agriculture Organization (1996):

$$q = \left(\frac{A_1}{A_2}\right)^{\frac{1}{t_2 - t_1}} - 1, \quad (1)$$

where A_1 and A_2 are the land cover at time t_1 and t_2, respectively.

[2]www.clarklabs.org/terrset/land-change-modeler/

Wildfires

Past burned areas (>1 ha; 1985–2018) were analyzed as the main potential driver of land cover change in the Puelo River Basin. Burned area reconstruction in the Chilean portion of the basin was performed by applying an algorithm in Google Earth Engine (GEE) (Long et al., 2019). GEE is an open cloud computing platform for geospatial analysis that contains a public catalog of historical satellite images, topography, land cover and other environmental datasets (Gorelick et al., 2017). Taking advantage of the GEE big-data analysis platform, we develop a flexible workflow to reconstruct individual burned area for all fires reported since 1985. This approach processes Landsat images and generates historical burned areas by detecting the multi-temporal reflectance change (before and after the fire) of the Normalized Burn Ratio [NBR = (ρNIR - ρSWIR2)/(ρNIR + ρSWIR2)], which uses the difference between pre- and post-fire reflectance of the near-infrared band (ρNIR) and short-wavelength infrared band (ρSWIR2) extracted from satellite images (Key and Benson, 2003). High values of NBR indicate a burned area that allows the reconstruction of the fire scar in the landscape. All the necessary data are freely available at GEE. This process needs as initial data the ignition point and date, which were compiled by the Chilean National Forestry Corporation (CONAF, 2018). In the Argentinean portion of the basin, the burned areas were obtained directly from MODIS MCD64A1 monthly data (500 m; 2001–2019) and the program of Provincial Agricultural Services (1985–2000).

Statistical Analysis

Water Quality

Nutrient and DOM data were analyzed with a multivariate approach focused on identifying spatial-temporal patterns of coherence between streamflow and water quality variables. Nutrient, DOC, DIC, and DOM data derived from spectroscopic characterization (CDOM (m^{-1}), color (Pt) and PARAFAC components) were first tested and transformed to meet the normality requirement as appropriate. The relationship between nutrients and DOM variables and between samples from all the sites and campaigns was evaluated using a heatmap and a hierarchical clustering approach on the Euclidean distances of the data matrix (*ComplexHeatmap* package v1.10 for R; Gu et al., 2016), which identifies clusters among and within samples and variables.

A non-metric dimensional scaling (NMDS) was used on the Manhattan distance matrix of nutrient concentration (N-total, P-total, NH_4, NO_3, NO_2, and PO_4) and DOM quality descriptors (PARAFAC components, CDOM, ColorPt, and DOC concentration). NH_4 and NO_2 were excluded from the analysis as more than 70% of the cases were below the detection limit. The effect of having total P and PO_4 samples below the detection limit in 50 and 30% of the cases was evaluated and the detection limit value was used (Palarea-Albaladejo and Martín-Fernández, 2015). The relationship between the NMDS of nutrients and DOM quality descriptors and streamflow was assessed by fitting streamflow onto the ordination (*envfit* function) and the result was plotted on the ordination diagram. The significance

of the correlation was assessed through a Monte Carlo test (1,000 permutations). Additionally, the grouping of the factors "Campaign" and "Site" was visualized through hulls plotted for each group using the function *ordihull* and the average of the group scores for each hull (function *ordibar*). The area of those polygons was then tested against areas produced by randomized groups through a permutation test (1,000 permutations) using the function *ordiareatest*. The NMDS was generated by *MetaMDS* function. To assess the effect of the factors campaign and site on DOM quality descriptors, permutation analysis of variance (PERMANOVA; Anderson, 2001) was performed on the corresponding Manhattan dissimilarity matrix (*adonis2* function). All the analyses described above were performed using *stats* v4.1 and *vegan* v2.5 packages for R.

Hydrological Regime

Trends in the hydrological regime of the Puelo River were examined using the Indicators of Hydrologic Alteration software (IHA; Richter et al., 1996). Based on daily data, this tool calculates 33 hydrological metrics that characterize the intra- and inter-annual variability in streamflow conditions, including the magnitude, frequency, duration, timing, and rate of change of streamflow. The metrics were estimated at the Puelo River fluviometric station located near the mouth (PD in **Figure 1**). This station has the most extensive records in the basin and possibly the longest in western Patagonia (water years: 1950–2019). This station adequately represents the hydrological behavior of the streamflows recorded by stations located upstream in Chile (Pearson correlation > 0.95 for the Manso and Puelo Rivers before their confluence; **Figure 1**). Missing daily data were filled with linear regressions with upstream stations (<1% of total data). The magnitude and the significance of the trends were analyzed with the Sen's slope (Sen, 1968) and Mann-Kendall tests (Mann, 1945) (*trend* package v1.1 for R).

Cross-wavelet transform (XWT) and coherence (XWC) analyses were applied to identify significant changes in the association between time series of precipitation and streamflow (Grinsted et al., 2004; Cazelles et al., 2008). XWT evaluates when two time series oscillate in common periods and if there is temporal lag between the peaks of the oscillations, and XWC analyzes the strength of this association (in the form of a correlation and a significance level). A high coherence (∼correlation) between two series for a given oscillation frequency and time period implies that the two series oscillate in a common frequency, and also that the lag between the peaks of the oscillations is constant, which suggests an underlying causal mechanism (Grinsted et al., 2004). XWT was calculated from log (streamflow; PD station in **Figure 1**) or square-root (precipitation; station located near Puerto Montt city 41.5°S), transformed series to attain normality. XWC was calculated in the Undarius High Performance Computer cluster at the Catalan Institute for Water Research, using a Monte Carlo randomization technique as in Grinsted et al. (2004). After XWT and XWC calculations, time series were extracted from correlation and the phase relationship of the most prominent common periods of oscillation shared by the two-time series, and calculated annual means. All data points that did not correspond to statistically significant ($p < 0.05$) associations as identified during XWT were discarded. The correlation and phase relationship of the same common periods of oscillation were extracted for each season and year. All calculations were performed using the *biwavelet* package v0.20.19 for R.

Hydrologic Modeling of LCC

Land Cover Scenarios

The hydrological model aims to evaluate the hydrological impact of three different land cover scenarios (SC), projected to the year 2030 based on observed LCC (2001–2016) and historical burned area (1985–2019). The first scenario (SC-1) considered a matrix of transition probability generated from LCC from 2001 to 2016 in the CA-MARKOV Module of IDRISI Selva v17.0 software[3]. This stochastic model assumes that in a given period pixel persistence or change in either class is dependent only on the immediately previous state, not on historical changes (Zhang and Dai, 2007; Zhang et al., 2011). A cellular automaton model was used to spatialize the Markov model results. This model allowed assessing the spatial changes among pixels, assuming that the changes are dependent on the initial condition and neighboring pixels (Guan et al., 2011; Yang et al., 2012). A standard 5×5 contiguity filter type cellular automaton and a 14-year iteration were used to generate the projected land cover for 2030. The second scenario (SC-2) assumed that the zones most likely to be burned are those where wildfires have been previously occurred. Under this assumption, SC-2 replaced SC-1 land cover with burned areas in those places where wildfires have occurred historically (1985–2019). Finally, the third scenario (SC-3) added to SC-2 new burned areas according to a 2 km buffer around the main lakes and urban or touristic spots, since most of the fires have been recorded in the vicinity of these places [see section "Land Cover Change (LCC)"]. The areas affected by wildfires were considered as bare land in the modeling process in order to evaluate the most extreme hydrological condition. This was the most recurrent condition detected during the post-fire analysis of LCC [see section "Land Cover Change (LCC)"]. Finally, the land cover classes were grouped into six categories: forest (primary, secondary, stunted, and exotic tree plantations), shrubland, grassland, bare land (including urban areas), water body, and snow and ice.

Hydrological Model WEAP

The three land cover scenarios for 2030 were simulated in the WEAP hydrological model (Water Evaluation and Planning; Yates et al., 2005), considering the same climatic conditions for each. The WEAP model, previously used in Chile (e.g., Vicuña et al., 2012; Chadwick et al., 2020; Barría et al., 2021), is a semi-distributed model that represents the relevant hydrological processes using empirical functions that describe the distribution of water in two soil water storages (root and deep storage). In this regard, the snow accumulation and snowmelt are based on the degree-day method, and the potential evapotranspiration (PET) was calculated with the Penman-Monteith equation. As a final output, the streamflow composition of each simulated river

[3]www.clarklabs.org

corresponds to the sum of surface runoff, interflow and baseflow. See Yates et al. (2005) for more details on the equations of the conceptual model.

The WEAP model was previously calibrated and validated for a monthly time step by Aguayo et al. (2021) using the corrected atmospheric products of section "Hydrology and Climate" (period 2000–2019). In this approach, the Puelo River Basin was divided into nine sub-basins (green squares in **Figure 1**), which were subdivided into different hydrological units according to their elevation and land cover type (baseline year 2001). The model reached a Modified Kling-Gupta Efficiency (Kling et al., 2012) of 0.83 and 0.74 for the calibration (2000–2010) and validation (2011–2019) stages, respectively (sub-basin PD in **Figure 1**). The model maintained high correlations (r = 0.78 ± 0.07) and dry biases (β = 0.93 ± 0.11) during the validation stage. These biases were mainly associated with high streamflow events when the probability of exceedance was less than 20%. In contrast, minimum annual streamflows were adequately simulated (r = 0.84). The simulated PET near the Reloncaví Fjord was similar to the time series recorded by an evaporation pan located in the same place (2002–2012; R^2 = 0.87, RMSE = 14 mm). Further details of the calibration/validation process and the parameter estimation can be found in Text S1 and Aguayo et al. (2021).

RESULTS

Water Quality in the Land-Ocean Interface

Nitrogen, phosphorus, dissolved carbon, and iron measured during the six field campaigns in the Puelo River Basin had very low concentrations (**Figure 3** and **Supplementary Table 2**) which are characteristic of well-conserved basins previously reported in southern Chile (**Supplementary Table 3**). In river samples (P1 to P4, Manso and Ventisquero), total nitrogen, phosphorus, dissolved carbon and iron concentration were mostly < 60 μg N L^{-1}, < 10 μg P L^{-1}, < 3.8 mg C L^{-1} and < 10 μg Fe L^{-1}. In contrast, the Reloncaví Fjord had mostly 3–15 times higher mean N, P, C and Fe concentrations (160–400 μg N L^{-1}, 27–74 μg P L^{-1}, 6–13 mg C L^{-1}, 22–26 μg Fe L^{-1}) which also increased remarkably by a factor of three from surface to 25 m depth (**Figure 3** and **Supplementary Table 2**). High values of total dissolved carbon in the fjord corresponded to the inorganic fraction; DOC concentrations were comparable across samples (**Supplementary Table 2**). The Ventisquero (V1) and Manso Rivers (M1) presented different mean values from those found by site in Puelo River's mainstem (**Supplementary Table 2**). The Ventisquero River showed the lowest mean total N and dissolved C concentration (<30 μg N L^{-1} and < 2,14 mg C L^{-1}), thus diluting nutrient concentrations of the mainstem after their confluence. Manso River transported higher nutrient loads, especially TP, leading to increases in P3 (**Figure 3**, **Supplementary Figure 1**, and **Supplementary Table 2**).

The NMDS separated the samples according to their origin of fjord versus basin and into the different sampling campaigns (**Figure 4** and **Supplementary Figure 1**; stress = 0.159). The first dimension was related, on the positive side, to protein-like DOM components, and with nutrients and DIC on the negative side. Fjord samples (F1 and F8) appeared grouped independently of the sampling campaign, and related to nutrients. The fjord's surface layer samples (1 m, F1) appear between the deeper fjord samples (8 m, F8) and the basin samples. The second dimension of the NMDS separated the basin samples by

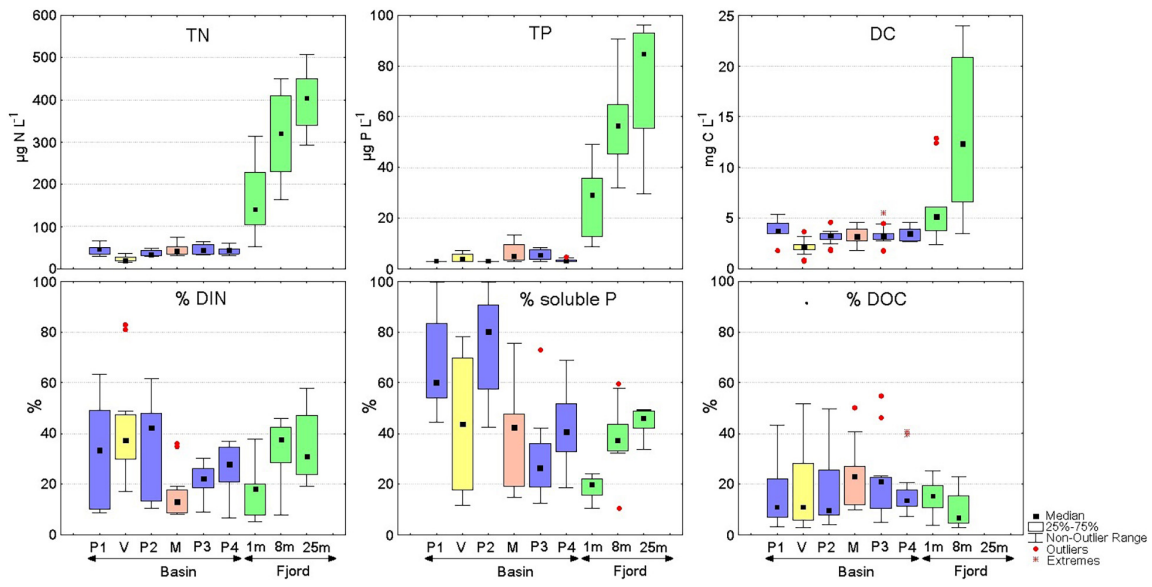

FIGURE 3 | Upper panel: Total nitrogen (TN), total phosphorus (TP) and total dissolved carbon (DC) concentrations measured in the Puelo River (P1-P4), Ventisquero River (V), Manso River (M) and Reloncaví Fjord at three depths (n = 12). Lower panel: Percentage of dissolved inorganic nitrogen (DIN), soluble phosphorous and dissolved organic carbon (DOC) with respect to the concentrations of the upper panel.

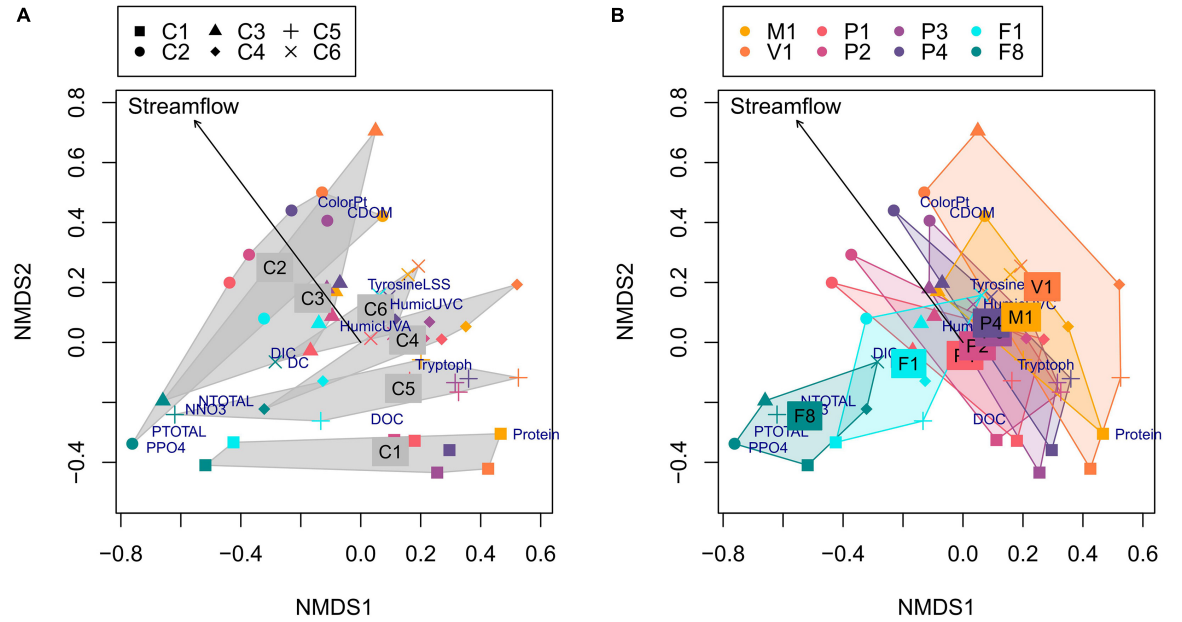

FIGURE 4 | Non-metric dimensional scaling (NMDS) ordination of all samples based on nutrients and DOM descriptors (symbol colors indicate the different sampling sites and shapes show the different campaigns). Labels indicate the nutrients and DOM descriptors. The left panel **(A)** shows hulls for the Campaign groups, labeled at the position of the average group scores. All the hulls except or C3 were significantly smaller than those produced by random groups. The right panel **(B)** shows hulls for the Site groups, labeled at the position of the average group scores. Only the hull for F8 is significantly smaller than those produced by random groups (see **Supplementary Table 4**). The arrow corresponds to streamflow values fitted to the ordination (r^2 = 0.1902, p = 0.01).

their different campaigns based mainly on DOM descriptors. Thus this dimension represents a gradient from colored and humic to protein-like DOM. C2 (Aug. 19) samples presented colored DOM, while those from C1 (May 19) had protein-like DOM. The remaining campaigns appeared ordered in the intermediate values of that second dimension. Streamflow appeared significantly fit to the NMDS ordination (r^2 = 0.19, p = 0.009), with higher streamflow conditions related to positive values of the second axis. Thus, these conditions (**Figure 2**) contribute with humic and colored materials (as in August, 2019), while low streamflows corresponded to higher arrival of protein-like materials from the basin (as in May, 2018). Fjord samples from 1 m are grouped together with Puelo River samples for each campaign. The permutation test for the size of the ordination hulls for campaign show that all the campaigns except C3 had smaller areas than random groups, while the test for sites shows that only F8 had a smaller area than random groups (**Supplementary Table 4**). In agreement with this, the PERMANOVA analysis of nutrients and DOM showed that both campaign and site had a significant effect (**Table 2**; FCampaign = 5.98, FSite = 10.32, p = 0.001 in both cases), although the effect of site was weaker when nutrients were excluded (**Table 2**; FSite = 3.26, p = 0.005, FCampaign = 10.12, p = 0.001).

Natural Flow Regime

Puelo River observational records analysis showed trends in magnitude, timing, duration, and change rate of streamflow (**Supplementary Table 1** and **Figure 5**). The streamflow recorded during summer and autumn showed statistically significant decreasing trends (summer in color palette of **Figure 5A**). The most affected months were January (−6% decade^{-1}; p < 0.001), February (−6% decade^{-1} p < 0.001), March (−4% decade^{-1}; p < 0.05) and May (−9% decade^{-1}; p < 0.05). The magnitude of such trends was also reflected in the Flow Duration Curve for the 1950–1979 and 1990–2019 periods (**Figure 2**). Inter-annual hydrological variability also showed significant changes associated with extreme conditions. Minimum annual streamflows for time windows of 7, 30, and 90 days showed statistically significant trends (**Supplementary Table 1** and **Figure 5A**). The timing of the maximum annual peak streamflow also changed. Only 10% of the years between 1950 and 1990 recorded the peak outside of the autumn or winter. In contrast, since 1990 this percentage has increased to 40% (p < 0.05; **Figure 5B**), and it has become more frequent to observe them in spring. Furthermore, the duration of the high streamflows registered a significant decrease (0.3 days decade^{-1}; color palette of **Figure 5B**). Finally, there were also significant trends in the streamflow fall rate (negative differences between consecutive values; **Supplementary Table 1**). The anomalies in the natural flow regime have coincided with the SAM trend (**Figure 5C**). In recent decades, the SAM positive phase has coincided with very warm ENSOs, which has favored extreme drought conditions in Northwestern Patagonia (e.g., 1998 and 2016 in **Figure 5**). This is not expected, considering that El Niño conditions tend to promote the negative phase of SAM, thus producing a negative correlation between their indices at interannual time-scales (L'Heureux and Thompson, 2006; Ding et al., 2012).

TABLE 2 | PERMANOVA analysis of (a) nutrients (N-total, P-total, NO_3, NO_2, and PO_4) and (b) DOM quality descriptors (PARAFAC components, CDOM, ColorPt, and DOC concentration), with sites and campaigns as factors.

(a) Nutrients	Df	SS	MS	Pseudo-F	P (perm)
Campaign	5	155.2	0.445	7.99	0.001***
Site	5	95.8	0.275	4.93	0.002**
Residual	25	97.1	0.278		
Total	35	348.1	1.000		
(b) DOM	**Df**	**SS**	**MS**	Pseudo-F	P(perm)
Campaign	5	168.7	0.466	10.1	0.001***
Site	7	76.1	0.210	3.23	0.008**
Residual	35	116.7	0.322		
Total	47	361.6	1.000		

*Df, degrees of freedom; SS, sum of squares; MS, mean sum of squares; Pseudo-F, F value by permutation, P(perm), p-values. ** < 0.01, *** < 0.001.*

The cross-wavelet transform and coherence analyses suggested shifts in the response of streamflow to precipitation events during the last decades (**Figure 6**). Beyond the expected year-to-year variability of the correlation (color) and lag (arrows) between streamflow and precipitation at short periods of oscillation (period from weeks to ∼3 months; **Figure 6A**), the analysis showed a significant common oscillation at 180 days (**Figure 6B**), corresponding to the relationship of precipitation peak during early winter and the streamflow peaks during early winter and late spring. For the oscillation at a period of 180 days, a significant increase (tau = 0.224, $p < 0.05$) of the lag between precipitation and streamflow was apparent (**Figure 6C**), from oscillations mostly around phase (lag ∼ 0, i.e. oscillations are synchronous) during the 1970s, to average lags around 20 days (and up to ∼50 days) during the last decade (i.e. streamflow peak had a lag of ∼20 days with respect to the precipitation peak), which is consistent with **Figure 5B**. This indicated that years with the prominent streamflow peak during spring are becoming more frequent. The correlation between the time-series at the period of oscillation of 180 days substantially decreased over years, showing longer lags between precipitation and streamflow (**Figure 6C**). This interpretation is also supported by the correlation between precipitation and streamflow oscillations analyzed at a period of 1 year, which shows consistently high correlation during the last decades (**Figure 6B**). This is expected if the double streamflow peak during winter-spring simplifies to a single peak, which would correlate better with the prominent precipitation peak during winter.

Land Cover Change (LCC)

The overall accuracy for satellite image classification was 85.3% for 2001 and 88.7% for 2016. The highest accuracy (except for water and bare soil) was achieved in primary forests (2001: 84.6%; 2016: 87.1%). The lowest values of accuracy corresponded to shrubland in 2001 and 2016 (76.6 and 81.8%, respectively). Land cover classification showed that 55% of the Puelo River Basin was covered by native forest in 2001 (**Figure 7c** and **Table 3**). Native forest cover rises to 77% without considering the water bodies and high elevated areas of bare land and snow. Other important classes were shrubland (13.5%) and bare land (18.7%) (**Tables 1**, **3**).

Land cover change analysis showed that 91.2% of the total area remained unchanged in the 2001–2016 period (**Figure 7a** and **Table 3**). The main changes corresponded to the increase of secondary forest (+3.7% yr^{-1}), shrubland (+0.2% yr^{-1}) and bare land (+0.5% yr^{-1}) (annual rate of change; **Table 3**). Secondary forest recovery was concentrated in areas with reduced human activity (e.g., Ventisquero River basin; **Figure 7a**). In contrast, the degradation processes associated with the loss of primary forest were located in the Turbio and Epuyén river valleys, where historical wildfires were concentrated (**Figures 7A,B**). Although exotic tree plantations and urban areas represented a minimum area in 2016, these land cover classes reported the highest annual rates of change (7.0 and 5.4%, respectively; **Table 3**).

The reconstruction of the burned area in the Puelo River Basin showed that 649.6 km^2 (7.1% of the basin) were affected by 74 wildfires between 1985 and 2019 (**Figure 7b** and **Table 1**). Of this total, 43 records occurred in Chile (109 km^2) and 31 in Argentina (539 km^2). Only 15 wildfires accumulated 88% of the total burned area (>10 km^2). Of these, only one occurred before 1995 (**Table 1**). The largest wildfires in Chile and Argentina occurred in the surroundings of Tagua-Tagua Lake (1998; 39 km^2) and Puelo Lake (2015; 129 km^2), respectively.

Hydrological Response to LCC

The three land cover scenarios projected toward the year 2030 showed LCC of different magnitude. SC-1 will decrease in primary (−1.1%) and stunted forest (−0.4%) (**Table 3**). SC-2 will add 524 km^2 of bare land in areas historically affected by wildfires (1985–2019) to SC-1, which affected mainly native forest areas (148 km^2), shrubland (197 km^2) and grasslands (24 km^2) (**Figure 7b** and **Table 3**). Finally, SC-3 will add 1,192 km^2 of possible burned areas to SC-2 according to a 2 km buffer around the principal lakes (**Figure 7d** and **Table 3**). Despite the extreme conditions assumed by this scenario, the native forest will decrease from 55.2 to 45.7%, while the bare land will increase from 18.7 to 31.6% (**Table 3**).

The decrease in vegetation cover shown by the three scenarios (e.g., native forest, shrubland) consistently reduced ET, and

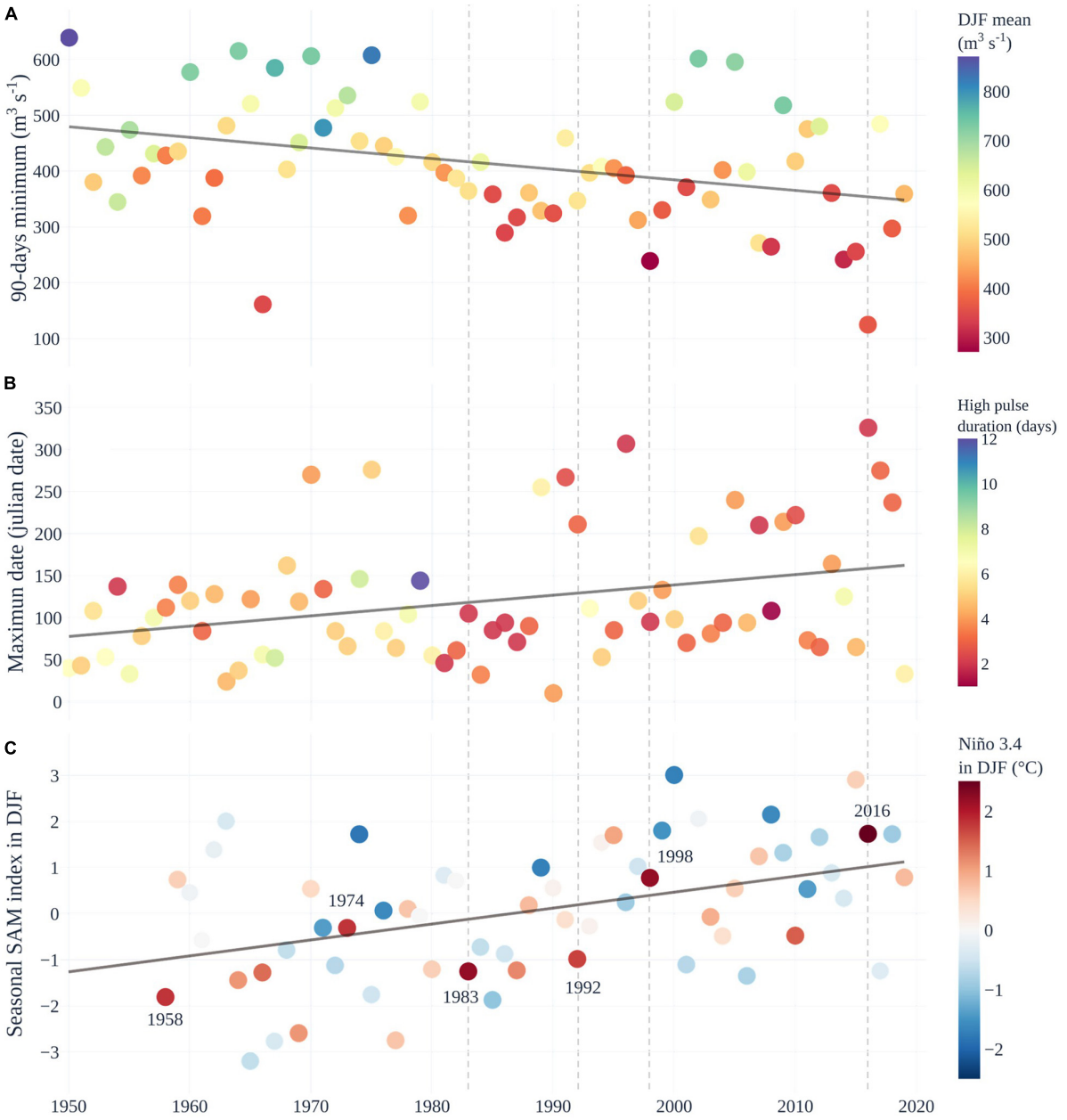

FIGURE 5 | Natural streamflow regime trends of the Puelo River and the climatic context. **(A)** Minimum annual streamflow in a 90-day window. The color palette in **(A)** represents the average streamflow during the summer season (DJF period). **(B)** Julian date of the maximum annual streamflow and high pulse duration (defined by 75th percentile; color palette). The first Julian day corresponds to the first day of the water year (April 1). **(C)** Southern Annular Mode (SAM) index during DJF as in Marshall (2003). The color palette represents the Niño 3.4 index during DJF of the HadISST1 data set. The segmented vertical lines indicate the main ENSO events.

altered internal hydrological processes (**Figure 8**). Reduced vegetation promotes changes in surface hydrological response, reducing infiltration rates and increasing surface runoff. Lower infiltration reduces subsurface flow and percolation into deep storage, which in turn controls base flow. Note that the base flow dominated the streamflow composition during the baseline period (2000–2019) with values of 40 ± 9% (**Figure 8**).

The magnitude of the hydrological response varied according to the scenarios, from non-significant changes (SC-1) to slight changes (SC-3) (**Figure 8**). Note that snow accumulation remained constant in **Figure 8**, since the climatic forcing does not change in the land cover scenarios. Regardless of the scenario evaluated, surface runoff and ET showed the greatest changes (**Figure 8**). Under the worst-case scenario (SC-3), the winter season recorded the largest projected changes in streamflow composition. In this season, the base flow, interflow and runoff showed changes relative to the baseline period of −2.0, −2.4, and 8.6%, respectively (**Figure 8**). Despite the seasonal

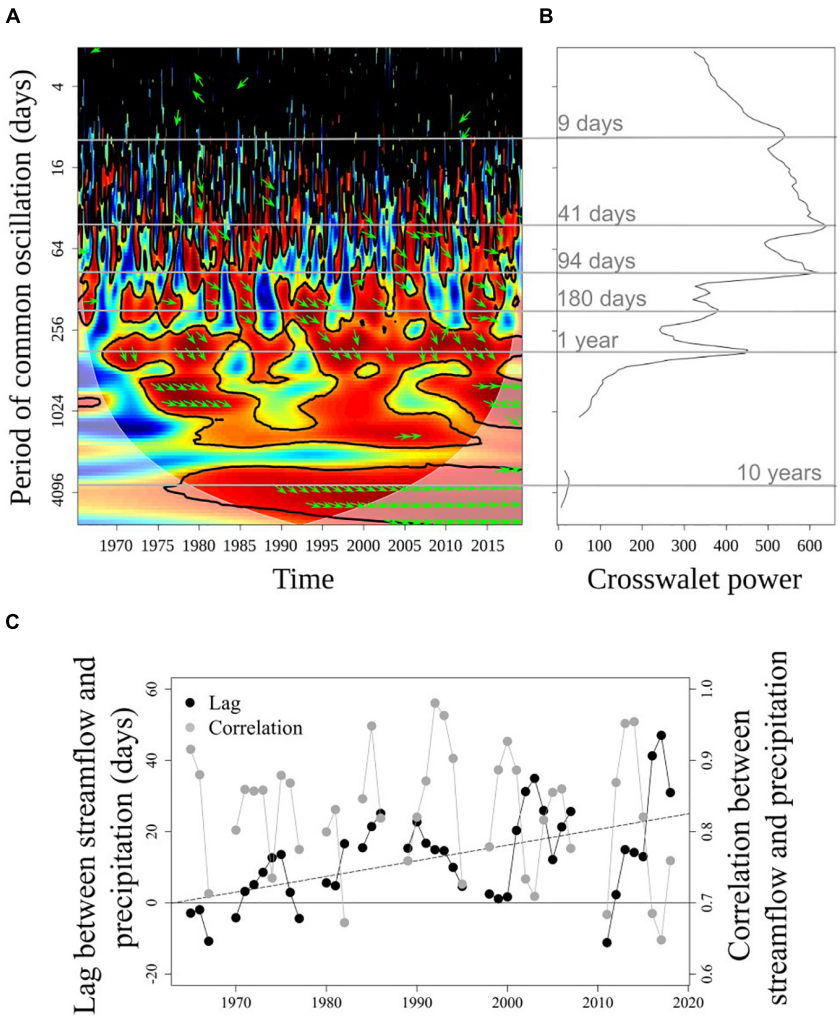

FIGURE 6 | Cross-wavelet transform and coherence analyses for the precipitation (in Puerto Montt) and streamflow time series (PD in **Figure 1**). **(A)** Cross-wavelet coherence plot, with significant regions delimited with a thick continuous line. Red colors denote high correlation. Shaded area is the cone of influence, where interpretations should be cautious. **(B)** Global cross-wavelet power showing the main periods of common oscillation. **(C)** Temporal lag (in days respect the precipitation series) and correlation between precipitation and streamflow analyzed at a period of 180 days. The dashed line is a linear trend for the lag, while the correlation did not show a significant trend. In panels b and c non-significant periods, lags, and correlations are not shown.

changes in hydrological processes, the same scenario indicated an average annual increase of only 1.1% of freshwater input to the Reloncaví Fjord.

DISCUSSION

This study illustrates the importance of water availability and quality of Puelo River Basin as the main freshwater input to the Reloncaví Fjord system. We show that the hydrology of the Puelo River has changed over time, with major shifts in magnitude (lower flows in summer and autumn), duration (minimum annual streamflows), timing (more floods in spring), and frequency (fewer prolonged floods). Concentrations of nitrogen and phosphorus must be highlighted as some of the lowest recorded for temperate rivers, highlighting the relatively pristine nature of the basin. The analysis of spectroscopic DOM descriptors and DOC concentration showed that streamflow and hydrological moment drive DOM composition in the hydrological network. The freshwater inputs from the Puelo River are fundamental to the haline stratification of the Reloncaví Fjord and the dilution of nutrients in the upper brackish layer. Wildfires have been the main driver of land cover change (LCC) in the past. Future LCC projections will reduce the evapotranspiration and subsurface flow, increasing the surface runoff, which will result in slight seasonal changes in freshwater inputs to the fjord. This study highlights the need for large coastal basins with near-reference conditions as indicators, sentinels or model systems for evaluating how could affect future scenarios of global environmental change affecting freshwater inputs (including volume, seasonal, and water quality) in fjord systems of Patagonia.

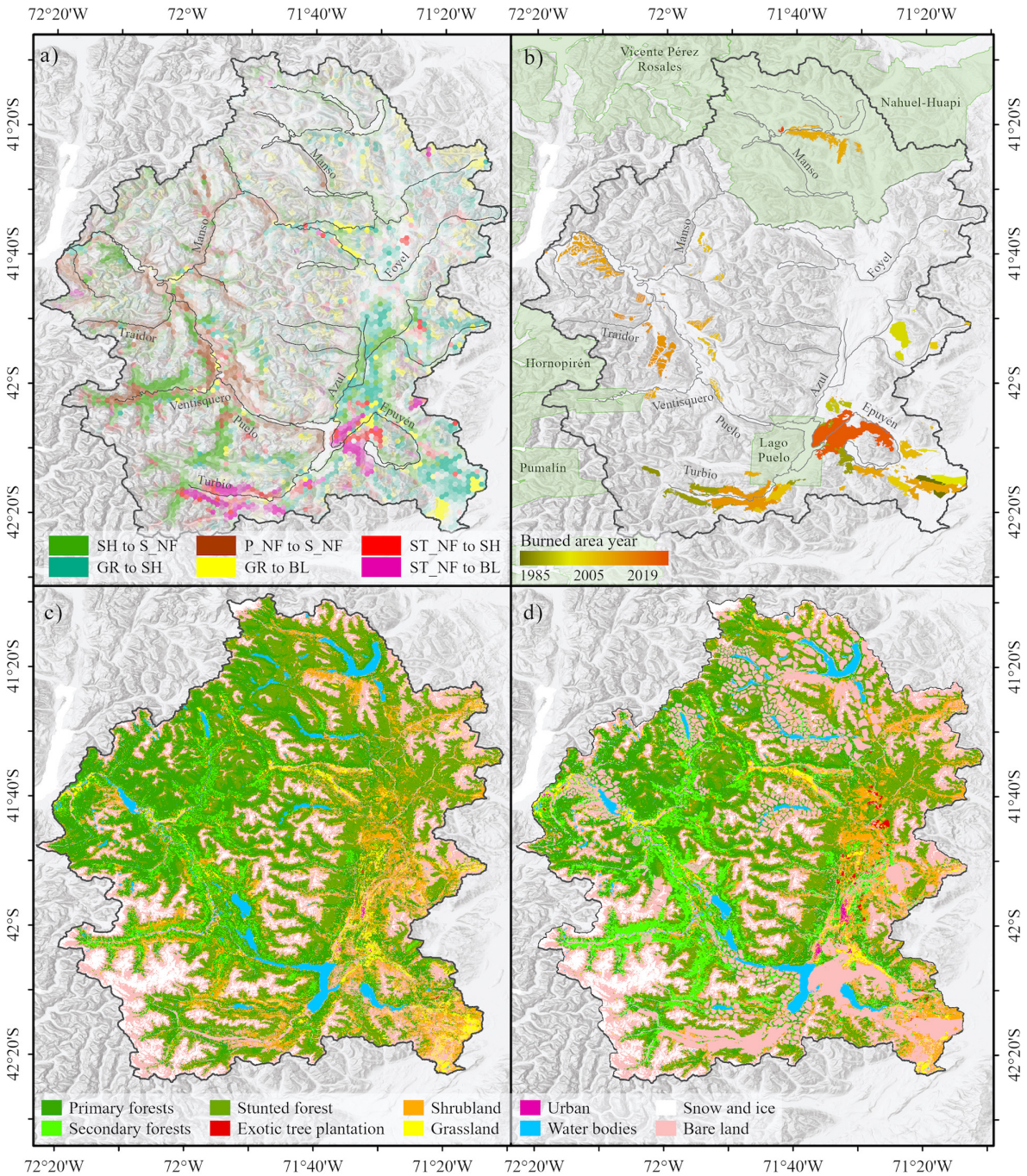

FIGURE 7 | (a) Land cover change in the Puelo River Basin during the 2001–2016 period. The colors in panel **(a)** indicate the six major land cover transitions (74% of the total changes). P_NF, Primary native forests; S_NF, Secondary native forest; ST_NF, Stunted native forest; SH, Shrubland; GR, Grassland; BL, Bare land. **(b)** Historical burned area (1985–2019). **(c)** Land cover in 2001. **(d)** Land cover in 2030 (SC-3), This scenario considered SC-1, the historically burned area in **(b)** and buffer areas around the main lakes and urban or touristic spots.

Natural Flow Regime and Freshwater Quality

Nutrient concentrations in the Puelo River drainage network across seasons are in the lower range of previously reported values for rivers in southern Chile (**Supplementary Table 3**; Oyarzun et al., 1997, 2004; Godoy et al., 1999, 2001; Perakis and Hedin, 2002; Oyarzún and Huber, 2003; Little et al., 2008), and elsewhere (de la Crétaz and Barten, 2007). Nutrient concentrations in the Reloncaví Fjord are much higher than those from the Puelo River. Therefore, the low concentration of N and P in these freshwater

TABLE 3 | Land cover in the Puelo River Basin in 2001, 2016 and 2030 (under the three scenarios).

Land-use cover	Area (%)					Rate of change (% yr^{-1})	
	2001	2016	2030 (SC-1)	2030 (SC-2)	2030 (SC-3)	2001–2016 (Historical)	2016–2030 (SC-1)
Native forest	55.2%	55.0%	53.6%	51.7%	45.7%	−0.03%	−0.17%
Primary forest	25.7%	23.9%	20.1%	19.3%	16.1%	−0.5%	−1.1%
Secondary forest	3.5%	6.1%	9.9%	9.2%	8.6%	3.7%	3.2%
Stunted forest	26.0%	25.0%	23.6%	23.3%	20.9%	−0.3%	−0.4%
Exotic tree plant.	0.1%	0.1%	0.3%	0.3%	0.3%	7.0%	5.5%
Shrubland	13.5%	14.0%	14.5%	12.2%	11.8%	0.2%	0.2%
Grassland	4.0%	2.2%	2.5%	2.2%	2.1%	−4.0%	0.8%
Urban	0.0%	0.1%	0.1%	0.1%	0.1%	5.4%	1.7%
Water bodies	2.7%	2.7%	2.7%	2.7%	2.7%	–	–
Snow and ice	5.8%	5.8%	5.8%	5.8%	5.8%	–	–
Bare land	18.7%	20.1%	20.5%	25.0%	31.6%	0.5%	0.1%

The annual rate of change was determined according to the formula proposed by FAO (1996). Total native forest cover is the sum of primary, secondary and stunted forests.

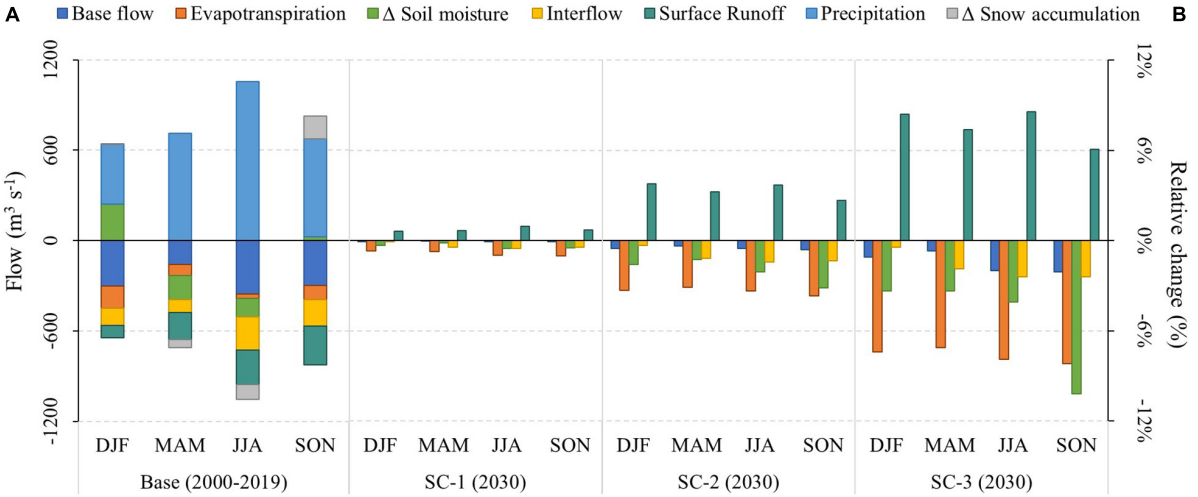

FIGURE 8 | (A) Hydrological balance of the Puelo River Basin using the WEAP model previously calibrated by Aguayo et al. (2021) (2000–2019; sub-basin PD in **Figure 1**). Positive flows (precipitation, soil moisture depletion and snowmelt) represent inflows of water to the basin. Negative flows represent accumulations (as soil moisture or snowpack) or outflows (evapotranspiration, surface runoff, interflow and base flow) from the basin. Note that storages can have a positive or negative sign depending on if they accumulate ($\Delta < 0$) or release water ($\Delta > 0$). **(B)** Relative changes of the hydrological processes for each scenario in relation to the same process during the baseline period. Each scenario represents different land covers in the year 2030. SC-1 projected land cover considering the changes that occurred in the period 2001–2016. SC-2 replaced SC-1 land cover with burned areas in those places where wildfires have occurred historically (1985–2019). SC-3 added to SC-2 new burned areas according to a 2 km buffer around the main lakes and urban areas.

inputs of the Puelo River may play a significant role in the coastal dynamics, influencing the upper layer of the Reloncaví Fjord. Clearly it can be stated out that the enhanced concentrations of dissolved and total fractions of N, P and Fe reported in the fjord are unlikely to be caused by the Puelo River input, as its nutrient and Fe content were always below the fjord samples. Therefore, it can only be speculated what other sources are responsible for the higher N, P and Fe concentration in the fjord; diffuse input from coastal sides, in-sea contamination from salmon farming and others. The NMDS and PERMANOVA analysis showed that nutrients present stronger differences between the fjord and the basin samples than DOM composition and the fjord's surface layer (1 m, mainly fresh and brackish water) nutrient concentrations are between the deeper fjord samples (measured at 8 and 25 m depth in the fjord) and the basin samples (**Supplementary Table 2**). This upper layer can limit the exchanges with deeper layers mostly of oceanic origin (González et al., 2013; Torres et al., 2014). This fjord has likely been more resilient to additional nutrient inputs (salmon farming; Soto et al., 2019) due to both the dilution role of freshwater input and rates of water turnover (Pinilla et al., 2020). Future scenarios of streamflow reduction might reduce water turnover in the fjord and enhance local eutrophication conditions. Hence the pristine conditions of freshwater input could provide important ecosystem services to maintain the resilience of the Reloncaví Fjord ecosystem to global environmental change.

NMDS based on nutrients, spectroscopic DOM descriptors and DOC concentrations (**Figure 4**) shows that streamflow and hydrological conditions drive DOM composition in freshwater. A closer examination of the origin of DOM from the Puelo River to the Reloncaví Fjord during the low streamflow period illustrates the fragile balance between hydrology and biogeochemical function of the river-fjord system. The PERMANOVA result, with both campaign and site being significant, does not allow us to present hydrology as the only control of DOM quality, but this result together with the NMDS sample clustering leads us to conclude that (i) seasonality and streamflow play a major role in it, (ii) the two major tributaries M1 and V1 contribute with low nutrient concentrations and very variable DOM quality (**Figure 4** and **Supplementary Table 4**).

High streamflow conditions during winter are related to humic and colored DOM, in agreement with behavior as a passive pipe; terrestrial DOM is transferred from soils to streams, and then rapidly transported toward the ocean without significant alteration (Raymond et al., 2016; Casas-Ruíz et al., 2020). In contrast, during low streamflow conditions we found an increase in protein-like DOM sources from degraded peptide material (Fellman et al., 2010) coming from the Puelo River Basin. This is likely due to the disconnection of lateral channel processes in the drainage network resulting in longer water residence time, and a large proportion of DOM from autochthonous sources (Casas-Ruiz et al., 2016; Catalán et al., 2016). However, we found a significant effect of site on DOM quality, and we expect some sections of the Puelo River drainage network to have a disproportionate influence on DOM quality and ultimately on the different layers of the Reloncaví Fjord. In order to constrain the link between hydrology and DOC concentration and DOM quality better, we encourage future studies to trace both the hydrograph and concentration response on a finer temporal scale and especially during extreme hydrologic conditions, as those may lead to especially harmful conditions in the fjord.

While our results help to understand the effect that the interplay between hydrological change and LCCs has on DOM composition, it is still unclear whether the relatively small LCC occurring in the Puelo River Basin have sufficient potential to affect fjord-level processes significantly. Targeting compounds at the molecular level (Coppola et al., 2018) might be key to identify the legacy of wildfires in these aquatic systems further. For example, increases in riverine export of dissolved black carbon have been found decades after wildfires in Brazil's Atlantic forest (Dittmar et al., 2012). Changes in the composition of riverine organic matter can alter carbon cycling in fjords due to shifts in both sedimentation rates and light penetration (Ward et al., 2017). However, even considering the constraints of our study, based on the high proportion of native forest in the Manso sub-basin, the projected LCC may reduce the DOM inputs from terrestrial vegetation (colored and typically aromatic) in the Reloncaví Fjord. This could lead to reduced flocculation and sedimentation in the coastal waters (Raymond and Spencer, 2015).

Recent hydrological shifts imply that the routing of water in the basin is undergoing profound changes. Considering the pristine nature of the basin, this also may have measurable yet unknown consequences for the export of DOC and nutrients from soils to rivers, and ultimately for the fjord. Although most studies focus on temperate, boreal and artic regions, it is well known that changes in hydrological regimes influence the export of DOC in relatively undisturbed basins (Winterdahl et al., 2016; Baek et al., 2019; Connolly et al., 2020). Unfortunately, our short-term study in terms of water chemistry cannot illuminate this issue, and there are no long-term records of organic matter and nutrient export from Patagonian basins to support claims related to changes in hydrological regimes. However, there is evidence from other regions that DOM export from snow-melt has a different chemical signature than exports from other flow paths (Burns et al., 2016). Furthermore, changes in timing and magnitude of streamflow in the region represent shifts in natural hydrological regimes (Poff et al., 1997; Poff, 2018), and could have additional biological implications in river networks and fjord ecosystems of this region. For example, the predicted shift in the hydrology of the Puelo River might increase the importance of autochthonous sources and decrease the transport of DOM from humic-like terrestrial sources reaching the fjord, except during storm episodes. Considering the relevance of organic carbon and nutrient exports for the ecological dynamics of the fjord and the expected hydrological changes in the future, understanding how this hydrological shift impacts constituent export from the basin should be a research priority.

Wildfires Are the Main Drivers of Land Cover Changes

The native forest cover in the Puelo River Basin (primary, secondary and stunted forests) showed an annual deforestation rate of 0.03%, with more than 90% of the basin area remaining unchanged during the period 2001–2016 (**Table 3**). As in Gowda et al. (2012), urban areas and exotic tree plantation had a marginal negative net contribution to forest cover throughout the period. However, these land cover classes reported the highest annual rates of change (7 and 5.4%, respectively, **Table 3**). The low LCC rate demonstrates the good conservation status of the Puelo River basin, differing from the values described for south-central Chile (33–42°S), an area that has been subjected to major LCC and is experiencing an annual rate of forest loss ranging between 0 and 5.8% (Miranda et al., 2017). Also the LCC ranges of the Puelo River basin are in the lower range of northwestern Patagonia, where Echeverría et al. (2012) reported an annual deforestation rate close to 1.0% (1985–1999 vs. 1999–2007).

According to our results, wildfires are main drivers of LCC in the Puelo River Basin. The frequency of fires in northwestern Patagonia peaked in the late nineteenth century, due to widespread burning and clearing of forests by European settlers. Fire frequency declined dramatically around 1910 due to the cessation of intentional fires; it has remained low due to current fire suppression (Kitzberger and Veblen, 1999; Veblen et al., 1999). In this study, the historical reconstruction of burned areas in the Puelo River Basin shows that 649.6 km^2 were affected by 74 wildfires between 1985 and 2019 (**Figure 7** and **Table 1**). Mundo et al. (2013) reported a strong negative association

between the density of fire ignitions and their distance to cities in this region (<5 km). This is consistent with the human origin of the fires in the Puelo River Basin, where most of wildfires have occurred around national parks, lakes and urban areas. Although the annual area burned in the Puelo River Basin has not changed over time, more than 90% of wildfires larger than 10 km^2 occurred after 1995. Climate trends might facilitate the spread of large wildfires, which added to the high fuel content in the region could increase the frequency of larger wildfires (Kitzberger and Veblen, 1999; González et al., 2018; Urrutia-Jalabert et al., 2018). In comparable mountain systems from western North America there is a strong link between wildfire activity and climate oscillations (Trouet et al., 2006; Holden et al., 2018).

Synergistic Hydrological Effects Between Climate and LCC

The three LCC scenarios showed changes of different magnitude in the Puelo River landscape. If current LCC trends continue (SC-1), native forest will decrease by 1.6% (relative value for 2001–2030), while if LCC intensifies due to potential wildfires (SC-3), native forest could decrease by up to 9.5% by 2030 (**Table 3**). Under these scenarios, bare land, the most recurrent land cover class after wildfires (**Figure 7**), would increase by 1.8 and 12.9%, respectively (**Table 3**). According to the WEAP model, these land cover transitions promote reductions in infiltration rates, which in turn reduce subsurface flow and percolation into deep storage (**Figure 8**). Reduced percolation can lead to a reduction in base flow, the dominant streamflow component of the Puelo River (40 ± 9%). Consistent with other hydrologic modeling in mountain systems (Havel et al., 2018), other processes observed in the hydrologic response were an increase in surface runoff and a decrease in evapotranspiration. The hydrologic response varied according to the scenario and remained similar between seasons. In the worst scenario for winter (SC-3), the hydrological model predicts changes of −2.0%, −2.4% and 8.6% on the base flow, interflow and runoff, respectively. The magnitude of projected changes is comparable to a deforestation scenario in the Vergara River Basin (Stehr et al., 2010), but lower than what was reported in south-central Chile, where changes in LCC are relatively more drastic and different (intensive forestry; Aguayo et al., 2016; Barrientos et al., 2020; Martínez-Retureta et al., 2020).

The hydrological simulations forced by LCC scenarios were an order of magnitude lower than the previous projections forced by the climate change scenarios. According to dendrochronological reconstructions, recent climate trends are unprecedented in the last centuries (e.g., SAM in **Figure 5C**; Villalba et al., 2012; Morales et al., 2020), which has been evident in the precipitation and temperature of northwestern Patagonia (Pabón-Caicedo et al., 2020). Recently, Aguayo et al. (2021) showed that temperature in northwestern Patagonia has increased during the whole year, but mainly in summer (0.3 ± 0.1°C decade^{-1}). In contrast, precipitation has decreased mainly during the autumn (−8 ± 8% decade^{-1}) and winter (−4 ± 9% decade^{-1}). Based on these climate trends, recent hydrological modeling in northwestern Patagonia projects an increase in the frequency of severe droughts during summer and autumn months (Aguayo et al., 2019, 2021; Pessacg et al., 2020). Lower streamflow conditions during summer are likely due to higher evapotranspiration (Ellenburg et al., 2018), and lower snow accumulation in snow-dominated regions (Barnett et al., 2005). Timing of the streamflow annual peaks have also changed in the Puelo River Basin, migrating from winter to less prolonged spring peaks. The increasing lag between precipitation and streamflow seasonally (from synchronous peaks to a lag of ∼50 days) suggests a shift in the peak streamflow timing (**Figure 6**). We hypothesize that the lower precipitation recorded in winter (maximum daily precipitation), together with a greater height of the 0°C isotherm in spring, allows the maximum annual streamflow to occur in spring.

The importance of various hydrological stressors depends on the local climatic, geographic and hydrological conditions, and the respective future trajectories (e.g., Davis et al., 2015; Yang et al., 2017; Chanapathi and Thatikonda, 2020). Hydrological projections for LCC and climate scenarios show opposite directions in the Puelo River Basin. Considering a moderate emissions scenario to the year 2030 (Shared Socio-economic Pathway Two), Aguayo et al. (2021) projected streamflow changes of −15, −18, 8, and 2% to DJF, MAM, JJA and SON, respectively (multi-model mean for 2020–2040 vs. 2000–2019). These values are an order of magnitude larger than those projected by LCC, since the projected climate trend for NP is one of the largest in the world (Cook et al., 2020). For example, Barría et al. (2021) recently determined that the relative impact of the climate factor is more than 10 times larger than the impact of the observed LLC changes in the Aculeo Lake balance (Central Chile; 33°S). Although these results may discourage conservation, Galleguillos et al. (2021) reported that conservative scenarios focused on native forest protection and restoration could partially mitigate the effect of climate change in Mediterranean basins. Future efforts should focus on understanding the hydrological role of different vegetation cover (e.g., Milkovic et al., 2019), under changing climatic conditions in northwestern Patagonia.

Long-Term Hydrological Trends Are Changing the Fjord System

Changes in climate ultimately result in modified trends of surface hydrology. During the last decades, the Puelo River regime showed a clear trend toward longer and more intense hydrological droughts, with major shifts in magnitude (lower flows in summer and autumn), duration (minimum annual streamflows), timing (more floods in spring), and frequency (fewer prolonged floods) (**Figure 5**). The trends in magnitude were consistent with those previously reported. Recently, Aguayo et al. (2021) showed a decreasing streamflow mainly during autumn (−6% ± 3% decade^{-1}) and summer (−5% ± 2% decade^{-1}) for most of the rivers of northwestern Patagonia. As a result of climate change, these results invite understanding the influence of the Puelo River as a non-stationary driver of the Reloncaví Fjord.

Changes in the natural flow regime during extreme climatic conditions, like during ENSO event in summer and autumn

(e.g., Valle-Levinson et al., 2007; León-Muñoz et al., 2018), could influence the occurrence of anomalous oceanographic events in the Reloncaví Fjord. The reduction in freshwater input drives the weakening of ocean stratification in the upper layer, allowing vertical advection of saline, less oxygenated and nutrient-rich waters (Valle-Levinson et al., 2007). These mechanisms have the potential to affect the production of mussels (*Mytilus chilensis*) and salmon (*Salmo salar* and *Onchorhynchus* spp.) in aquaculture facilities (Soto et al., 2019). For example, an increase in the salinity of the fjord's surface layer can alter environmental conditions that minimize the impacts of caligidosis (sea louse) in salmon (Montory et al., 2018). León-Muñoz et al. (2018) reported that the severe drought during 2016 (the lowest streamflow in 70 years) generated the appropriate conditions for a record harmful algae bloom in northwestern Patagonia. As a consequence, the mortality of salmon in a few days was comparable to the mortality that all salmon farming usually experiences in 2 years (US$ 800 million). This extreme event is also a relevant threat to mussel culture (Chávez et al., 2019; Soto et al., 2020). Coastal sites with high input of freshwater seem to ensure better mussel seed provision, survival and capture, apparently because the wild mussel populations providing the seeds are more successful at lower salinities (Molinet et al., 2015, Molinet et al., 2021). Therefore, the decreasing trend in freshwater input to the Reloncaví Fjord during drought years, and the changes in its timing, could be compromising the future of these two industries (Soto et al., 2020).

CONCLUSION

The Puelo River streamflow showed non-stationary conditions with clear trends toward longer and more intense droughts. Several indicators of the natural flow regime also showed significant trends, such as the timing of the maximum annual peak streamflow, the duration of high streamflows and the streamflow fall rate. Despite the recent increase in wildfires in recent decades, more than 90% of the total area maintained its land cover during the period 2001–2016. Considering these trends, the hydrological simulations based on land cover scenarios toward the year 2030 will slightly influence hydrological processes (e.g., surface runoff, evapotranspiration), and therefore the hydrological regime of the Puelo River will be mostly modulated by climate trends. These climate trends would imply hydrological changes in the opposite direction to those forced by the LCC scenarios. The combined effect of both hydrological stressors and potential decline in water quality (increase in nutrients) is a call for more robust data monitoring and analysis of both drivers. For example, it is essential to advance in the understanding the hydrological role of different vegetation covers under warmer and drier climatic conditions in northwestern Patagonia.

Nutrient concentrations in the drainage network are in the lower range of previously reported values for rivers in southern Chile, and are 3–15 times lower than in the fjord. As result, the fjord′s surface layer limits the exchanges with deeper water layers mostly of oceanic origin. Future decreases in freshwater input might reduce water turnover in the fjord and enhance local eutrophication conditions. Coastal sites with high freshwater input support large-scale salmon aquaculture and ensure better mussel seed survival. Considering the relevance of organic carbon and nutrient exports, understanding how this hydrological shift influences the export of basin constituents warrants further research. For example, to trace both the hydrograph and concentration response on a finer temporal scale during extreme hydrologic conditions, as these may lead to anomalous and extreme events in the fjord (e.g., harmful alga bloom, hypoxia events). This study provides baseline information about present and future threats relevant to the potential of "losing the freshwater-dependent resilience" of the Reloncaví Fjord to future global environmental change. More research is still needed to understand better the influence of water availability and quality on the biogeochemistry, food webs and ecosystem services provided by this river-fjord complex.

DATA AVAILABILITY STATEMENT

The datasets generated for this study can be found in the Zenodo repository (https://doi.org/10.5281/zenodo.4604929). This repository contains hydro-climatic observations, gridded products of precipitation and temperature, land cover for different periods, and the reconstruction of burned areas. The raw data from CHIRPSv2, MODIS MOD11C3, and ERA5 can be found at www.chc.ucsb.edu/data/chirps (last access: June 12, 2021), https://lpdaac.usgs.gov/products/mod11c3v006 (last access: June 12, 2021), and www.ecmwf.int/en/forecasts/datasets/reanalysis-datasets/era5 (last access: June 12, 2021), respectively.

AUTHOR CONTRIBUTIONS

JL-M: conceptualization, methodology, validation, investigation, formal analysis, and writing—original draft. RA and CC: methodology, investigation, software, formal analysis, data curation, visualization, and writing—reviewing and editing. NC: methodology, investigation, software, formal analysis, and writing—reviewing and editing. RM: software, formal analysis, and writing—reviewing and editing. SW and JN: investigation, formal analysis, and writing—reviewing and editing. DS, IA, and AM: writing—reviewing and editing. All authors contributed to the article and approved the submitted version.

FUNDING

This research was supported by projects ANID—FONDECYT: N°11170768 "Potential effects of land use change on fjords of western Patagonia under climate change scenarios" and Interdisciplinary Center for Aquaculture Research (FONDAP INCAR 15110027, ANID). RA was supported by ANID PFCHA/DOCTORADO NACIONAL/2019—21190544. RM and NC participated trough the project C-HydroChange (CGL2017-86788-C3-2-P) of the Spanish Ministry of Economy and Competitiveness.

ACKNOWLEDGMENTS

We thank Directorate of Water (DGA), Meteorological Directorate of Chile (DMC), and the Sub-Secretariat of Water Resources of Argentina (SRHA) for their role in collecting data.

SUPPLEMENTARY MATERIAL

The Supplementary Material for this article can be found online at: https://www.frontiersin.org/articles/10.3389/fmars.2021.628454/full#supplementary-material

REFERENCES

Aguayo, M., Stehr, A., and Link, O. (2016). Respuesta hidrológica de una cuenca de meso escala frente a futuros escenarios de expansión forestal. *Rev. Geogr. Norte Gd.* 65, 197–214. doi: 10.4067/S0718-34022016000300010

Aguayo, R., León-Muñoz, J., Garreaud, R., and Montecinos, A. (2021). Hydrological droughts in the southern Andes (40–45°S) from an ensemble experiment using CMIP5 and CMIP6 models. *Sci. Rep.* 11:5530. doi: 10.1038/s41598-021-84807-4

Aguayo, R., León-Muñoz, J., Vargas-Baecheler, J., Montecinos, A., Garreaud, R., Urbina, M., et al. (2019). The glass half-empty: climate change drives lower freshwater input in the coastal system of the Chilean Northern Patagonia. *Clim. Change* 155, 417–435. doi: 10.1007/s10584-019-02495-6

Alvarez-Garreton, C., Lara, A., Boisier, J. P., and Galleguillos, M. (2019). The impacts of native forests and forest plantation on water supply in Chile. *Forests* 10:473. doi: 10.3390/f10060473

American Public Health Association (2005). *Standard Methods for the Examination of water and wastewater*, 21st Edn. Washington, DC: American Public Health Association.

Anderson, M. J. (2001). A new method for non parametric multivariate analysis of variance. *Austral. Ecol.* 26, 32–46.

Arblaster, J. M., and Meehl, G. A. (2006). Contributions of external forcings to southern annular mode trends. *J. Clim.* 19, 2896–2905. doi: 10.1175/JCLI3774.1

Astorga, A., Moreno, P., and Reid, B. (2018). Watersheds and trees fall together: an analysis of intact forested watersheds in southern Patagonia (41–56° S). *Forests* 9:385. doi: 10.3390/f9070385

Aufdenkampe, A. K., Mayorga, E., Raymond, P. A., Melack, J. M., Doney, S. C., Alin, S. R., et al. (2011). Riverine coupling of biogeochemical cycles between land, oceans, and atmosphere. *Front. Ecol. Environ.* 9:14. doi: 10.1890/100014

Baek, S., Jeon, J., Lee, H., Park, J., and Cho, K. (2019). investigating influence of hydrological regime on organic matters characteristic in a korean watershed. *Water* 11:512. doi: 10.3390/w11030512

Barbier, E. B., Hacker, S. D., Kennedy, C., Koch, E. W., Stier, A. C., and Silliman, B. R. (2011). The value of estuarine and coastal ecosystem services. *Ecol. Monogr.* 81, 169–193. doi: 10.1890/10-1510.1

Barnett, T. P., Adam, J. C., and Lettenmaier, D. P. (2005). Potential impacts of a warming climate on water availability in snow-dominated regions. *Nature* 438, 303–309. doi: 10.1038/nature04141

Barría, P., Chadwick, C., Ocampo-Melgar, A., Galleguillos, M., Garreaud, R., Díaz-Vasconcellos, R., et al. (2021). Water management or megadrought: what caused the Chilean Aculeo Lake drying? *Reg. Environ. Chang.* 21:19.

Barrientos, G., Herrero, A., Iroumé, A., Mardones, O., and Batalla, R. J. (2020). Modelling the effects of changes in forest cover and climate on hydrology of headwater catchments in south-central Chile. *Water* 12:1828. doi: 10.3390/w12061828

Beck, H. E., Zimmermann, N. E., McVicar, T. R., Vergopolan, N., Berg, A., and Wood, E. F. (2018). Present and future Köppen-Geiger climate classification maps at 1-km resolution. *Sci. Data* 5:180214. doi: 10.1038/sdata.2018.214

Boisier, J. P., Alvarez-Garreton, C., Cordero, R. R., Damiani, A., Gallardo, L., Garreaud, R. D., et al. (2018). Anthropogenic drying in central-southern Chile evidenced by long-term observations and climate model simulations. *Elem. Sci. Anthr.* 6:74. doi: 10.1525/elementa.328

Boisramé, G. F. S., Thompson, S. E., Tague, C., and Stephens, S. L. (2019). Restoring a natural fire regime alters the water balance of a sierra nevada catchment. *Water Resour. Res.* 55, 5751–5769. doi: 10.1029/2018WR024098

Burns, M. A., Barnard, H. R., Gabor, R. S., McKnight, D. M., and Brooks, P. D. (2016). Dissolved organic matter transport reflects hillslope to stream connectivity during snowmelt in a montane catchment. *Water Resour. Res.* 52, 4905–4923. doi: 10.1002/2015WR017878

Casas-Ruíz, J. P., Spencer, R. G. M., Guillemette, F., Schiller, D., Obrador, B., Podgorski, D. C., et al. (2020). Delineating the continuum of dissolved organic matter in temperate river networks. *Global Biogeochem. Cycles* 34:e2019GB006495. doi: 10.1029/2019gb006495

Casas-Ruiz, J. P., Tittel, J., von Schiller, D., Catalán, N., Obrador, B., Gómez-Gener, L., et al. (2016). Drought-induced discontinuities in the source and degradation of dissolved organic matter in a Mediterranean river. *Biogeochemistry* 127, 125–139.

Castillo, M. I., Cifuentes, U., Pizarro, O., Djurfeldt, L., and Caceres, M. (2016). Seasonal hydrography and surface outflow in a fjord with a deep sill: the Reloncaví fjord. *Chile. Ocean Sci.* 12, 533–534. doi: 10.5194/os-12-533-2016

Catalán, N., Marcé, R., Kothawala, D. N., and Tranvik, L. J. (2016). Organic carbon decomposition rates controlled by water retention time across inland waters. *Nat. Geosci.* 9, 501–504. doi: 10.1038/ngeo2720

Cazelles, B., Chavez, M., Berteaux, D., Ménard, F., Vik, J. O., Jenouvrier, S., et al. (2008). Wavelet analysis of ecological time series. *Oecologia* 156, 287–304.

Chadwick, C., Gironás, J., Barría, P., Vicuña, S., and Meza, F. (2020). Assessing reservoir performance under climate change. when is it going to be too late if current water management is not changed? *Water* 13:64. doi: 10.3390/w13010064

Chanapathi, T., and Thatikonda, S. (2020). Investigating the impact of climate and land-use land cover changes on hydrological predictions over the Krishna river basin under present and future scenarios. *Sci. Total Environ.* 721:137736. doi: 10.1016/j.scitotenv.2020.137736

Chávez, C., Dresdner, J., Figueroa, Y., and Quiroga, M. (2019). Main issues and challenges for sustainable development of salmon farming in Chile: a socio-economic perspective. *Rev. Aquac.* 11, 403–421. doi: 10.1111/raq.12338

CONAF (2018). *Estadísticas Históricas De Incendios Forestales en Chile*. Available online at: https://www.conaf.cl/incendios-forestales/incendios-forestales-en-chile/estadisticas-historicas/ (accessed January 6, 2020).

CONAF, CONAMA, and Birf. (1999). *Catastro y Evaluación De Los Recursos Vegetacionales Nativos De Chile. Informe nacional con Variables Ambientales*. Santiago: Natural Resources Information Center (CIREN).

CONAF, and UACH. (2014). *Monitoreo De Cambios, Corrección Cartográfica Y Actualización Del Catastro De Recursos Vegetacionales Nativos de la Región de Los Lagos*. Santiago: Natural Resources Information Center (CIREN).

Connolly, C. T., Cardenas, M. B., Burkart, G. A., Spencer, R. G. M., and McClelland, J. W. (2020). Groundwater as a major source of dissolved organic matter to Arctic coastal waters. *Nat. Commun.* 11:1479. doi: 10.1038/s41467-020-15250-8

Cook, B. I., Mankin, J. S., Marvel, K., Williams, A. P., Smerdon, J. E., and Anchukaitis, K. J. (2020). Twenty-First Century Drought Projections in the CMIP6 Forcing Scenarios. *Earth's Futur.* 8, 1–20. doi: 10.1029/2019EF001461

Coppola, A. I., Wiedemeier, D. B., Galy, V., Haghipour, N., Hanke, U. M., Nascimento, G. S., et al. (2018). Global-scale evidence for the refractory nature of riverine black carbon. *Nat. Geosci.* 11, 584–588. doi: 10.1038/s41561-018-0159-8

Cuevas, J. G., Soto, D., Arismendi, I., Pino, M., Lara, A., and Oyarzún, C. (2006). Relating land cover to stream properties in southern Chilean watersheds: trade-off between geographic scale, sample size, and explicative power. *Biogeochemistry* 81, 313–329. doi: 10.1007/s10533-006-9043-5

Dávila, P. M., Figueroa, D., and Müller, E. (2002). Freshwater input into the coastal ocean and its relation with the salinity distribution off austral Chile (35-55°s). *Cont. Shelf Res.* 22, 521–534. doi: 10.1016/S0278-4343(01)00072-3

Davis, J., O'Grady, A. P., Dale, A., Arthington, A. H., Gell, P. A., Driver, P. D., et al. (2015). When trends intersect: The challenge of protecting freshwater ecosystems under multiple land use and hydrological intensification scenarios. *Sci. Total Environ.* 534, 65–78. doi: 10.1016/j.scitotenv.2015.03.127

de la Crétaz, A., and Barten, P. K. (2007). *Land Use Effects on Streamflow and Water Quality in the Northeastern United States*. Boca Raton, FL: CRC Press, doi: 10.1201/9781420008722.ch7

Desmit, X., Thieu, V., Billen, G., Campuzano, F., Dulière, V., Garnier, J., et al. (2018). Reducing marine eutrophication may require a paradigmatic change. *Sci. Total Environ.* 635, 1444–1466.

Díaz, P. A., Peréz-Santos, I., Álvarez, G., Garreaud, R., Pinilla, E., Díaz, M., et al. (2021). Multiscale physical background to an exceptional harmful algal bloom of Dinophysis acuta in a fjord system. *Sci. Total Environ.* 773:145621. doi: 10.1016/j.scitotenv.2021.145621

Ding, Q., Steig, E. J., Battisti, D. S., and Wallace, J. M. (2012). Influence of the tropics on the southern annular mode. *J. Clim.* 25, 6330–6348.

Dittmar, T., de Rezende, C. E., Manecki, M., Niggemann, J., Coelho Ovalle, A. R., Stubbins, A., et al. (2012). Continuous flux of dissolved black carbon from a vanished tropical forest biome. *Nat. Geosci.* 5, 618–622. doi: 10.1038/ngeo1541

Echeverria, C., Coomes, D., Salas, J., Rey-Benayas, J. M., Lara, A., and Newton, A. (2006). Rapid deforestation and fragmentation of Chilean Temperate Forests. *Biol. Conserv.* 130, 481–494. doi: 10.1016/j.biocon.2006.01.017

Echeverría, C., Newton, A., Nahuelhual, L., Coomes, D., and Rey-Benayas, J. M. (2012). How landscapes change: Integration of spatial patterns and human processes in temperate landscapes of southern Chile. *Appl. Geogr.* 32, 822–831. doi: 10.1016/j.apgeog.2011.08.014

Ellenburg, W. L., Cruise, J. F., and Singh, V. P. (2018). The role of evapotranspiration in streamflow modeling – An analysis using entropy. *J. Hydrol.* 567, 290–304. doi: 10.1016/j.jhydrol.2018.09.048

Ellison, D., Morris, C. E., Locatelli, B., Sheil, D., Cohen, J., Murdiyarso, D., et al. (2017). Trees, forests and water: cool insights for a hot world. *Glob. Environ. Chang.* 43, 51–61. doi: 10.1016/j.gloenvcha.2017.01.002

Eyring, V., Arblaster, J. M., Cionni, I., Sedláček, J., Perlwitz, J., Young, P. J., et al. (2013). Long-term ozone changes and associated climate impacts in CMIP5 simulations. *J. Geophys. Res. Atmos.* 118, 5029–5060. doi: 10.1002/jgrd.50316

Farías, L., Sanzana, K., Sanhueza-Guevara, S., and Yevenes, M. A. (2017). dissolved methane distribution in the reloncaví fjord and adjacent marine system during Austral Winter (41°–43° S). *Estuaries and Coasts* 40, 1592–1606. doi: 10.1007/s12237-017-0241-2

Fellman, J. B., Hood, E., and Spencer, R. G. M. (2010). Fluorescence spectroscopy opens new windows into dissolved organic matter dynamics in freshwater ecosystems: a review. *Limnol. Oceanogr.* 55, 2452–2462. doi: 10.4319/lo.2010.55.6.2452

Food and Agriculture Organization (1996). *Forest Resources Assessment 1990. Survey of Tropical Forest Cover and Study of Change Process*. Roma: Food and Agriculture Organization of the United Nations.

Fuentes, R., León-Muñoz, J., and Echeverría, C. (2017). Spatially explicit modelling of the impacts of land-use and land-cover change on nutrient inputs to an oligotrophic lake. *Int. J. Remote Sens.* 38, 7531–7550. doi: 10.1080/01431161.2017.1339928

Funk, C., Peterson, P., Landsfeld, M., Pedreros, D., Verdin, J., Shukla, S., et al. (2015). The climate hazards infrared precipitation with stations—a new environmental record for monitoring extremes. *Sci. Data* 2:150066. doi: 10.1038/sdata.2015.66

Galleguillos, M., Gimeno, F., Puelma, C., Zambrano-Bigiarini, M., Lara, A., and Rojas, M. (2021). Disentangling the effect of future land use strategies and climate change on streamflow in a Mediterranean catchment dominated by tree plantations. *J. Hydrol.* 595:126047. doi: 10.1016/j.jhydrol.2021.126047

Garreaud, R. (2018). Record-breaking climate anomalies lead to severe drought and environmental disruption in western Patagonia in 2016. *Clim. Res.* 74, 217–229. doi: 10.3354/cr01505

Godoy, R., Oyarzún, C., and Bahamondes, J. (1999). Flujos hidroquímicos en un bosque de Nothofagus pumilio en el Parque Nacional Puyehue, sur de Chile. *Rev. Chil. Hist. Nat.* 72, 579–594.

Godoy, R., Oyarzún, C., and Gerding, V. (2001). Precipitation chemistry in deciduous and evergreen Nothofagus forests of southern Chile under a low-deposition climate. *Basic Appl. Ecol.* 2, 65–72. doi: 10.1078/1439-1791-00037

González, H. E., Castro, L. R., Daneri, G., Iriarte, J. L., Silva, N., Tapia, F., et al. (2013). Land-ocean gradient in haline stratification and its effects on plankton dynamics and trophic carbon fluxes in Chilean Patagonian fjords (47-50°S). *Prog. Oceanogr.* 119, 32–47. doi: 10.1016/j.pocean.2013.06.003

González, H. E., Nimptsch, J., Giesecke, R., and Silva, N. (2019). Organic matter distribution, composition and its possible fate in the Chilean North-Patagonian estuarine system. *Sci. Total Environ.* 657, 1419–1431. doi: 10.1016/j.scitotenv.2018.11.445

González, M. E., Gómez-González, S., Lara, A., Garreaud, R., and Díaz-Hormazábal, I. (2018). The 2010-2015 Megadrought and its influence on the fire regime in central and south-central Chile. *Ecosphere* 9:e02300. doi: 10.1002/ecs2.2300

Gorelick, N., Hancher, M., Dixon, M., Ilyushchenko, S., Thau, D., and Moore, R. (2017). Google Earth Engine: planetary-scale geospatial analysis for everyone. *Remote Sens. Environ.* 202, 18–27. doi: 10.1016/j.rse.2017.06.031

Gowda, J. H., Kitzberger, T., and Premoli, A. C. (2012). Landscape responses to a century of land use along the northern Patagonian forest-steppe transition. *Plant Ecol.* 213, 259–272. doi: 10.1007/s11258-011-9972-5

Grinsted, A., Moore, J. C., and Jevrejeva, S. (2004). Application of the cross wavelet transform and wavelet coherence to geophysical time series. *Nonlinear Process. Geophys.* 11, 561–566. doi: 10.5194/npg-11-561-2004

Gu, Z., Eils, R., and Schlesner, M. (2016). Complex heatmaps reveal patterns and correlations in multidimensional genomic data. *Bioinformatics* 32, 2847–2849. doi: 10.1093/bioinformatics/btw313

Guan, D., Li, H., Inohae, T., Su, W., Nagaie, T., and Hokao, K. (2011). Modeling urban land use change by the integration of cellular automaton and Markov model. *Ecol. Modell.* 222, 3761–3772. doi: 10.1016/j.ecolmodel.2011.09.009

Havel, A., Tasdighi, A., and Arabi, M. (2018). Assessing the hydrologic response to wildfires in mountainous regions. *Hydrol. Earth Syst. Sci.* 22, 2527–2550. doi: 10.5194/hess-22-2527-2018

Hernes, P. J., and Benner, R. (2003). Photochemical and microbial degradation of dissolved lignin phenols: Implications for the fate of terrigenous dissolved organic matter in marine environments. *J. Geophys. Res. Ocean.* 108:3291. doi: 10.1029/2002JC001421

Hersbach, H., Bell, B., Berrisford, P., Hirahara, S., Horányi, A., Muñoz-Sabater, J., et al. (2020). The ERA5 global reanalysis. *Q. J. R. Meteorol. Soc.* 146, 1999–2049. doi: 10.1002/qj.3803

Holden, Z. A., Swanson, A., Luce, C. H., Jolly, W. M., Maneta, M., Oyler, J. W., et al. (2018). Decreasing fire season precipitation increased recent western US forest wildfire activity. *Proc. Natl. Acad. Sci. U.S.A.* 115, E8349–E8357. doi: 10.1073/pnas.1802316115

Iriarte, J. L., González, H. E., Liu, K. K., Rivas, C., and Valenzuela, C. (2007). Spatial and temporal variability of chlorophyll and primary productivity in surface waters of southern Chile (41.5–43° S). *Estuar. Coast. Shelf Sci.* 74, 471–480. doi: 10.1016/j.ecss.2007.05.015

Iriarte, J. L., León-Muñoz, J., Marcé, R., Clément, A., and Lara, C. (2017). Influence of seasonal freshwater streamflow regimes on phytoplankton blooms in a Patagonian fjord. *New Zeal. J. Mar. Freshw. Res.* 51, 304–315. doi: 10.1080/00288330.2016.1220955

Iriarte, J. L., Pantoja, S., and Daneri, G. (2014). Oceanographic processes in chilean fjords of patagonia: from small to large-scale studies. *Prog. Oceanogr.* 129, 1–7. doi: 10.1016/j.pocean.2014.10.004

Iroumé, A., and Palacios, H. (2013). Afforestation and changes in forest composition affect runoff in large river basins with pluvial regime and Mediterranean climate. Chile. *J. Hydrol.* 505, 113–125. doi: 10.1016/j.jhydrol.2013.09.031

Jacob, B. G., Tapia, F. J., Daneri, G., Iriarte, J. L., Montero, P., Sobarzo, M., et al. (2014). Springtime size-fractionated primary production across hydrographic and PAR-light gradients in Chilean Patagonia (41-50°S). *Prog. Oceanogr.* 129, 75–84. doi: 10.1016/j.pocean.2014.08.003

Kamjunke, N., Nimptsch, J., Harir, M., Herzsprung, P., Schmitt-Kopplin, P., Neu, T. R., et al. (2017). Land-based salmon aquacultures change the quality and bacterial degradation of riverine dissolved organic matter. *Sci. Rep.* 7:43739. doi: 10.1038/srep43739

Key, C., and Benson, N. (2003). The normalized Burn Ratio (NBR): A Landsat TM Radiometric Measure of Burn Severity. US Geological Survey Northern Rocky Mountain Science Center. U.S. Department of the Interior, U.S. Geological Survey, Northern Rocky Mountain Science Center. Available online at: https://www.frames.gov/catalog/5860 (accessed January 6, 2020).

Khoury, S., and Coomes, D. A. (2020). Resilience of Spanish forests to recent droughts and climate change. *Glob. Chang. Biol.* 26, 7079–7098. doi: 10.1111/gcb.15268

Kitzberger, T., and Veblen, T. T. (1999). Fire-induced changes in northern Patagonian landscapes. *Landsc. Ecol.* 14, 1–15. doi: 10.1023/A:1008069712826

Kling, H., Fuchs, M., and Paulin, M. (2012). Runoff conditions in the upper Danube basin under an ensemble of climate change scenarios. *J. Hydrol.* 42, 264–277. doi: 10.1016/j.jhydrol.2012.01.011

Lara, A., Villalba, R., and Urrutia, R. (2008). A 400-year tree-ring record of the Puelo River summer-fall streamflow in the Valdivian Rainforest eco-region, Chile. *Clim. Change* 86, 331–356. doi: 10.1007/s10584-007-9287-7

León-Muñoz, J., Marcé, R., and Iriarte, J. L. (2013). Influence of hydrological regime of an Andean river on salinity, temperature and oxygen in a Patagonia fjord, Chile. *New Zeal. J. Mar. Freshw. Res.* 47, 515–528. doi: 10.1080/00288330.2013.802700

León-Muñoz, J., Urbina, M. A., Garreaud, R., and Iriarte, J. L. (2018). Hydroclimatic conditions trigger record harmful algal bloom in western Patagonia (summer 2016). *Sci. Rep.* 8:1330. doi: 10.1038/s41598-018-19461-4

L'Heureux, M. L., and Thompson, D. W. J. (2006). Observed Relationships between the El Niño–Southern oscillation and the extratropical zonal-mean circulation. *J. Clim.* 19, 276–287. doi: 10.1175/JCLI3617.1

Little, C., Lara, A., McPhee, J., and Urrutia, R. (2009). Revealing the impact of forest exotic plantations on water yield in large scale watersheds in South-Central Chile. *J. Hydrol.* 374, 162–170. doi: 10.1016/j.jhydrol.2009.06.011

Little, C., Soto, D., Lara, A., and Cuevas, J. G. (2008). Nitrogen exports at multiple-scales in a southern Chilean watershed (Patagonian Lakes district). *Biogeochemistry* 87, 297–309. doi: 10.1007/s10533-008-9185-8

Long, T., Zhang, Z., He, G., Jiao, W., Tang, C., Wu, B., et al. (2019). 30 m Resolution Global Annual Burned Area Mapping Based on Landsat Images and Google Earth Engine. *Remote Sens.* 11, 489. doi: 10.3390/rs11050489

Mages, M., Woelfl, S., Óvári, M., and Tümpling jun, W. v (2003). The use of a portable total reflection X-ray fluorescence spectrometer for field investigation. *Spectrochim. Acta Part B At. Spectrosc* 58, 2129–2138. doi: 10.1016/S0584-8547(03)00197-6

Mann, H. B. (1945). Nonparametric tests against trend. *Econometrica* 13:245. doi: 10.2307/1907187

Marshall, G. J. (2003). Trends in the Southern Annular Mode from Observations and Reanalyses. *J. Clim* 16, 4134–4143.

Martínez-Retureta, R., Aguayo, M., Stehr, A., Sauvage, S., Echeverría, C., and Sánchez-Pérez, J.-M. (2020). Effect of Land Use/Cover Change on the hydrological response of a southern center basin of Chile. *Water* 12:302. doi: 10.3390/w12010302

Milkovic, M., Paruelo, J. M., and Nosetto, M. D. (2019). Hydrological impacts of afforestation in the semiarid Patagonia: a modelling approach. *Ecohydrology* 12:e2113. doi: 10.1002/eco.2113

Milliman, J. D., and Farnsworth, K. L. (2011). *River Discharge to the Coastal Ocean*. Cambridge: Cambridge University Press, doi: 10.1017/CBO9780511781247

Miranda, A., Altamirano, A., Cayuela, L., Lara, A., and González, M. (2017). Native forest loss in the Chilean biodiversity hotspot: revealing the evidence. *Reg. Environ. Chang.* 17, 285–297. doi: 10.1007/s10113-016-1010-7

Miranda, A., Lara, A., Altamirano, A., Zamorano-Elgueta, C., Hernández, H. J., González, M. E., et al. (2018). Monitoreo de la superficie de los bosques nativos de Chile: un desafío pendiente. *Bosque (Valdivia)* 39, 265–275. doi: 10.4067/S0717-92002018000200265

Molinet, C., Astorga, M., Cares, L., Diaz, M., Hueicha, K., Marín, S., et al. (2021). Patrones de distribución vertical del suministro de larvas y spatfall de tres especies de Mytilidae en un fiordo chileno utilizado para el cultivo de mejillones: Insights for mussel spatfall efficiency. *Aquaculture* 535. doi: 10.1016/j.aquaculture.2021.736341

Molinet, C., Díaz, M., Arriagada, C., Cares, L., Marín, S., Astorga, M., et al. (2015). Spatial distribution pattern of Mytilus chilensis beds in the Reloncaví fjord: hypothesis on associated processes. *Rev. Chil. Hist. Nat.* 88:11. doi: 10.1186/s40693-015-0041-7

Montory, J. A., Cumillaf, J. P., Cubillos, V. M., Paschke, K., Urbina, M. A., and Gebauer, P. (2018). Early development of the ectoparasite Caligus rogercresseyi under combined salinity and temperature gradients. *Aquaculture* 486, 68–74. doi: 10.1016/j.aquaculture.2017.12.017

Morales, M. S., Cook, E. R., Barichivich, J., Christie, D. A., Villalba, R., LeQuesne, C., et al. (2020). Six hundred years of South American tree rings reveal an increase in severe hydroclimatic events since mid-20th century. *Proc. Natl. Acad. Sci. U.S.A.* 117, 16816–16823. doi: 10.1073/pnas.2002411117

Mundo, I. A., Wiegand, T., Kanagaraj, R., and Kitzberger, T. (2013). Environmental drivers and spatial dependency in wildfire ignition patterns of northwestern Patagonia. *J. Environ. Manage.* 123, 77–87. doi: 10.1016/j.jenvman.2013.03.011

Murphy, K. R., Butler, K. D., Spencer, R. G. M., Stedmon, C. A., Boehme, J. R., and Aiken, G. R. (2010). Measurement of Dissolved Organic Matter Fluorescence in Aquatic Environments: an interlaboratory comparison. *Environ. Sci. Technol.* 44, 9405–9412. doi: 10.1021/es102362t

Nimptsch, J., Woelfl, S., Kronvang, B., Giesecke, R., González, H. E., Caputo, L., et al. (2014). Does filter type and pore size influence spectroscopic analysis of freshwater chromophoric DOM composition? *Limnologica* 48, 57–64. doi: 10.1016/j.limno.2014.06.003

Nixon, S. W., and Buckley, B. A. (2002). "A strikingly rich zone"—Nutrient enrichment and secondary production in coastal marine ecosystems. *Estuaries* 25, 782–796. doi: 10.1007/BF02804905

Oyarzun, C., Campos, H., and Huber, A. (1997). Exportación de nutrientes en microcuencas con distinto uso del suelo en el sur de Chile (Lago Rupanco, X Región). *Rev. Chil. Hist. Nat.* 70, 507–519.

Oyarzun, C. E., Godoy, R., De Schrijver, A., Staelens, J., and Lust, N. (2004). Water chemistry and nutrient budgets in an undisturbed evergreen rainforest of southern Chile. *Biogeochemistry* 71, 107–123. doi: 10.1007/s10533-004-4107-x

Oyarzún, C. E., and Huber, A. (2003). Nitrogen export from forested and agricultural watersheds of southern Chile. *Gayana. Botánica* 60, 63–68. doi: 10.4067/S0717-66432003000100010

Pabón-Caicedo, J. D., Arias, P. A., Carril, A. F., Espinoza, J. C., Borrel, L. F., Goubanova, K., et al. (2020). Observed and projected hydroclimate changes in the andes. *Front. Earth Sci.* 8:61. doi: 10.3389/feart.2020.00061

Palarea-Albaladejo, J., and Martín-Fernández, J. A. (2015). zCompositions — R package for multivariate imputation of left-censored data under a compositional approach. *Chemom. Intell. Lab. Syst.* 143, 85–96. doi: 10.1016/j.chemolab.2015.02.019

Pantoja, S., Luis Iriarte, J., and Daneri, G. (2011). Oceanography of the Chilean Patagonia. *Cont. Shelf Res.* 31, 149–153. doi: 10.1016/j.csr.2010.10.013

Perakis, S. S., and Hedin, L. O. (2002). Nitrogen loss from unpolluted South American forests mainly via dissolved organic compounds. *Nature* 415, 416–419. doi: 10.1038/415416a

Pessacg, N., Flaherty, S., Solman, S., and Pascual, M. (2020). Climate change in northern Patagonia: critical decrease in water resources. *Theor. Appl. Climatol.* 140, 807–822. doi: 10.1007/s00704-020-03104-8

Pinilla, E., Soto, G., Soto-Riquelme, C., Venegas, O., Salas, P., and Cortes, J. (2020). *Determinación de las Escalas de Intercambio de Agua en Fiordos y Canales de la Región de Los Lagos y Región de Aysén del General Carlos Ibáñez del Campo*. Valparaiso: Instituto de Fomento Pesquero (IFOP), doi: 10.13140/RG.2.2.17813.65762

Poff, N. L. (2018). Beyond the natural flow regime? Broadening the hydro-ecological foundation to meet environmental flows challenges in a non-stationary world. *Freshw. Biol.* 63, 1011–1021. doi: 10.1111/fwb.13038

Poff, N. L., Allan, J. D., Bain, M. B., Karr, J. R., Prestegaard, K. L., Richter, B. D., et al. (1997). The natural flow regime. *Bioscience* 47, 769–784. doi: 10.2307/1313099

Quiñones, R. A., Fuentes, M., Montes, R. M., Soto, D., and León-Muñoz, J. (2019). Environmental issues in Chilean salmon farming: a review. *Rev. Aquac* 11, 375–402. doi: 10.1111/raq.12337

Raymond, P. A., Oh, N.-H., Turner, R. E., and Broussard, W. (2008). *Anthropogenically* enhanced fluxes of water and carbon from the Mississippi River. *Nature* 451, 449–452. doi: 10.1038/nature06505

Raymond, P. A., Saiers, J. E., and Sobczak, W. V. (2016). Hydrological and biogeochemical controls on watershed dissolved organic matter transport: pulse-shunt concept. *Ecology* 97, 5–16. doi: 10.1890/07-1861.1

Raymond, P. A., and Spencer, R. G. M. (2015). "Riverine DOM," in *Biogeochemistry of Marine Dissolved Organic Matter*, eds C. A. Carlson and D. A. Hansell (Amsterdam: Elsevier), 509–533. doi: 10.1016/B978-0-12-405940-5.00011-X

Rebolledo, L., Lange, C. B., Bertrand, S., Muñoz, P., Salamanca, M., Lazo, P., et al. (2015). Late Holocene precipitation variability recorded in the sediments of Reloncaví Fjord (41°S, 72°W), Chile. *Quat. Res.* 84, 21–36. doi: 10.1016/j.yqres.2015.05.006

Richter, B. D., Baumgartner, J. V., Powell, J., and Braun, D. P. (1996). A Method for assessing hydrologic alteration within ecosystems. *Conserv. Biol.* 10, 1163–1174. doi: 10.1046/j.1523-1739.1996.10041163.x

Rulli, M. C., and Rosso, R. (2007). Hydrologic response of upland catchments to wildfires. *Adv. Water Resour.* 30, 2072–2086. doi: 10.1016/j.advwatres.2006.10.012

Saldías, G. S., Sobarzo, M., and Quiñones, R. (2019). Freshwater structure and its seasonal variability off western Patagonia. *Prog. Oceanogr.* 174, 143–153. doi: 10.1016/j.pocean.2018.10.014

Segura, R., and Trincado, G. (2003). Cartografía digital de la Reserva Nacional Valdivia a partir de imágenes satelitales Landsat TM. *Bosque (Valdivia)* 24, 43–52. doi: 10.4067/S0717-92002003000200005

Sen, P. K. (1968). Estimates of the regression coefficient based on Kendall's Tau. *J. Am. Stat. Assoc.* 63:1379. doi: 10.2307/2285891

Sievers, H., and Silva, N. (2008). "Water masses and circulation in austral Chilean channels and fjords," in *Progress in the Oceanographic Knowledge of Chilean Interior Waters, from Puerto Montt to Cape Horn*, eds N. Silva and S. Palma (Valparaíso: Comité Oceanográfico Nacional - Pontificia Universidad Católica de Valparaíso), 53–58.

Silva, N., Vargas, C. A., and Prego, R. (2011). Land–ocean distribution of allochthonous organic matter in surface sediments of the Chiloé and Aysén interior seas (Chilean Northern Patagonia). *Cont. Shelf Res.* 31, 330–339. doi: 10.1016/j.csr.2010.09.009

Soto, D., León-Muñoz, J., Dresdner, J., Luengo, C., Tapia, F. J., and Garreaud, R. (2019). Salmon farming vulnerability to climate change in southern Chile: understanding the biophysical, socioeconomic and governance links. *Rev. Aquac.* 11, 354–374. doi: 10.1111/raq.12336

Soto, D., León-Muñoz, J., Molinet, C., Soria-Galvarro, Y., Videla, J., Opazo, D., et al. (2020). *Informe Mapas de riesgo ante el cambio climático Acuicultura, Proyecto ARClim. Centro de Ciencia del Clima y la Resiliencia y Centro de Cambio Global UC para el Ministerio del Medio Ambiente a traveìs de La Deutsche Gesellschaft für Internationale Zusammenarbeit (GIZ)*. (Chile, Ministerio del Medio Ambiente).

Stedmon, C. A., and Bro, R. (2008). Characterizing dissolved organic matter fluorescence with parallel factor analysis: a tutorial. *Limnol. Oceanogr. Methods* 6, 572–579. doi: 10.4319/lom.2008.6.572

Stehr, A., Aguayo, M., Link, O., Parra, O., Romero, F., and Alcayaga, H. (2010). Modelling the hydrologic response of a mesoscale Andean watershed to changes in land use patterns for environmental planning. *Hydrol. Earth Syst. Sci.* 14, 1963–1977. doi: 10.5194/hess-14-1963-2010

Torres, R., Reid, B., Frangópulos, M., Alarcón, E., Márquez, M., Häusermann, V., et al. (2020). Freshwater runoff effects on the production of biogenic silicate and chlorophyll-a in western Patagonia archipelago (50–51°S). *Estuar. Coast. Shelf Sci.* 241:106597. doi: 10.1016/j.ecss.2020.106597

Torres, R., Silva, N., Reid, B., and Frangopulos, M. (2014). Silicic acid enrichment of subantarctic surface water from continental inputs along the Patagonian archipelago interior sea (41-56°S). *Prog. Oceanogr.* 129, 50–61. doi: 10.1016/j.pocean.2014.09.008

Trouet, V., Taylor, A. H., Carleton, A. M., and Skinner, C. N. (2006). Fire-climate interactions in forests of the American Pacific coast. *Geophys. Res. Lett.* 33:L18704. doi: 10.1029/2006GL027502

Uribe, S. V., Estades, C. F., and Radeloff, V. C. (2020). Pine plantations and five decades of land use change in central Chile. *PLoS One* 15:e0230193. doi: 10.1371/journal.pone.0230193

Urrutia-Jalabert, R., González, M. E., González-Reyes, Á, Lara, A., and Garreaud, R. (2018). Climate variability and forest fires in central and south-central Chile. *Ecosphere* 9:e02171. doi: 10.1002/ecs2.2171

Valle-Levinson, A., Castro, L., Cáceres, M., and Pizarro, O. (2014). Twilight vertical migrations of zooplankton in a Chilean fjord. *Prog. Oceanogr.* 129, 114–124. doi: 10.1016/j.pocean.2014.03.008

Valle-Levinson, A., Sarkar, N., Sanay, R., Soto, D., and León, J. (2007). Spatial structure of hydrography and flow in a Chilean fjord, Estuario Reloncaví. *Estuaries Coasts* 30, 113–126. doi: 10.1007/BF02782972

Vargas, C. A., Martinez, R. A., San Martin, V., Aguayo, M., Silva, N., and Torres, R. (2011). Allochthonous subsidies of organic matter across a lake-river-fjord landscape in the Chilean Patagonia: implications for marine zooplankton in inner fjord areas. *Cont. Shelf Res.* 31, 187–201. doi: 10.1016/j.csr.2010.06.016

Veblen, T. T., Kitzberger, T., Raffaele, E., and Lorenz, D. C. (1999). "Fire History and Vegetation Changes in Northern Patagonia, Argentina," in *Fire and Climatic Change in Temperate Ecosystems of the Western Americas*, eds G. Montenegro, T. T. Veblen, T. W. Swetnam, and W. L. Baker (New York, NY: Springer-Verlag), 265–295. doi: 10.1007/0-387-21710-X_9

Vergara-Jara, M. J., DeGrandpre, M. D., Torres, R., Beatty, C. M., Cuevas, L. A., Alarcón, E., et al. (2019). Seasonal changes in carbonate saturation state and Air-Sea CO 2 fluxes during an annual cycle in a stratified-temperate Fjord (Reloncaví Fjord, Chilean Patagonia). *J. Geophys. Res. Biogeosci.* 124, 2851–2865. doi: 10.1029/2019JG005028

Vicuña, S., McPhee, J., and Garreaud, R. D. (2012). Agriculture vulnerability to climate change in a snowmelt-driven basin in semiarid Chile. *J. Water Resour. Plan. Manag.* 138, 431–441. doi: 10.1061/(ASCE)WR.1943-5452.0000202

Villalba, R., Lara, A., Masiokas, M. H., Urrutia, R., Luckman, B. H., Marshall, G. J., et al. (2012). Unusual Southern Hemisphere tree growth patterns induced by changes in the Southern Annular Mode. *Nat. Geosci.* 5, 793–798. doi: 10.1038/ngeo1613

Wan, Z., Hook, S., and Hulley, G. (2015). *MOD11C3 MODIS/Terra Land Surface Temperature/Emissivity Monthly L3 Global 0.05Deg CMG V006 [Data set]. NASA EOSDIS L. Process*. Oak Ridge, TEN: DAAC, doi: 10.5067/MODIS/MOD11C3.006

Ward, N. D., Bianchi, T. S., Medeiros, P. M., Seidel, M., Richey, J. E., Keil, R. G., et al. (2017). Where carbon goes when water flows: carbon cycling across the aquatic continuum. *Front. Mar. Sci.* 4:7. doi: 10.3389/fmars.2017.00007

Winterdahl, M., Laudon, H., Lyon, S. W., Pers, C., and Bishop, K. (2016). Sensitivity of stream dissolved organic carbon to temperature and discharge: Implications of future climates. *J. Geophys. Res. Biogeosci.* 121, 126–144. doi: 10.1002/2015JG002922

Wu, J., Wang, D., and Bauer, M. E. (2007). Assessing broadband vegetation indices and QuickBird data in estimating leaf area index of corn and potato canopies. *F. Crop. Res.* 102, 33–42. doi: 10.1016/j.fcr.2007.01.003

Yang, L., Feng, Q., Yin, Z., Wen, X., Si, J., Li, C., et al. (2017). Identifying separate impacts of climate and land use/cover change on hydrological processes in upper stream of Heihe River, Northwest China. *Hydrol. Process.* 31, 1100–1112. doi: 10.1002/hyp.11098

Yang, X., Zheng, X.-Q., and Lv, L.-N. (2012). A spatiotemporal model of land use change based on ant colony optimization, Markov chain and cellular automata. *Ecol. Modell.* 233, 11–19. doi: 10.1016/j.ecolmodel.2012.03.011

Yates, D., Sieber, J., Purkey, D., and Huber-Lee, A. (2005). WEAP21—A Demand-, Priority-, and preference-driven water planning model. *Water Int.* 30, 487–500. doi: 10.1080/02508060508691893

Yevenes, M. A., Lagos, N. A., Farías, L., and Vargas, C. A. (2019). Greenhouse gases, nutrients and the carbonate system in the Reloncaví Fjord (Northern Chilean Patagonia): Implications on aquaculture of the mussel, Mytilus chilensis, during an episodic volcanic eruption. *Sci. Total Environ.* 669, 49–61. doi: 10.1016/j.scitotenv.2019.03.037

Zhang, L., and Dai, S. (2007). Application of Markov model to environmental fate of phenanthrene in Lanzhou Reach of Yellow River. *Chemosphere* 67, 1296–1299. doi: 10.1016/j.chemosphere.2006.11.026

Zhang, R., Tang, C., Ma, S., Yuan, H., Gao, L., and Fan, W. (2011). Using Markov chains to analyze changes in wetland trends in arid Yinchuan Plain, China. *Math. Comput. Model.* 54, 924–930. doi: 10.1016/j.mcm.2010.11.017

Conflict of Interest: The authors declare that the research was conducted in the absence of any commercial or financial relationships that could be construed as a potential conflict of interest.